

# $\alpha$ -cluster correlations and symmetry breaking in light nuclei

Yoshiko Kanada-En'yo

*Department of Physics, Kyoto University, Kyoto 606-8502, Japan*

Yoshimasa Hidaka

*Theoretical Research Division, Nishina Center, RIKEN, Wako 351-0198, Japan*

$\alpha$ -cluster correlations in the ground states of  $^{12}\text{C}$  and  $^{16}\text{O}$  are studied. Because of the  $\alpha$  correlations, the intrinsic states of  $^{12}\text{C}$  and  $^{16}\text{O}$  have triangle and tetrahedral shapes, respectively. The deformations are regarded as spontaneous symmetry breaking of rotational invariance, and the resultant oscillating surface density is associated with a density wave (DW) state caused by the instability of Fermi surface with respect to a kind of  $1p$ - $1h$  correlations. To discuss the symmetry breaking between uniform density states and the oscillating density state, a schematic model of a few clusters on a Fermi gas core in a one-dimensional finite box was introduced. The model analysis suggests structure transitions from a Fermi gas state to a DW-like state via a BCS-like state, and to a Bose Einstein condensation (BEC)-like state depending on the cluster size relative to the box size. It was found that the oscillating density in the DW-like state originates in Pauli blocking effects.

## I. INTRODUCTION

Nuclear deformation is one of the typical collective motions in nuclear systems. It is known that ground states of nuclei often have static deformations in the intrinsic states, which are regarded as spontaneous symmetry breaking of the rotational invariance due to collective correlations. Needless to say, the broken symmetry in the intrinsic states is restored in nuclear energy levels, because total angular momenta are good quanta in energy eigenstates of the finite system. Not only normal deformations of axial symmetric quadrupole deformations but also triaxial, octupole, and super deformations have been attracting interests in these decades. To investigate those deformation phenomena mean-field approaches have been applied, in particular, for heavy mass nuclei.

In light nuclear systems, further exotic shapes due to cluster structures have been suggested. For instance, a triangle shape in  $^{12}\text{C}$  and a tetrahedral one in  $^{16}\text{O}$  have been discussed based on the cluster picture that  $^{12}\text{C}$  and  $^{16}\text{O}$  are considered to be  $3\alpha$  and  $4\alpha$  systems. In old days, to understand spectra of  $^{12}\text{C}$  and  $^{16}\text{O}$  non-microscopic  $\alpha$ -cluster models have been applied [1, 2]. From vibrations of the triangle structure of three  $\alpha$  particles and the tetrahedral one of four  $\alpha$ s, Wheeler has suggested the low-lying  $J = 3$  states in  $^{12}\text{C}$  and  $^{16}\text{O}$  [1], which are now considered to correspond to the lowest negative-parity states  $^{12}\text{C}(3_1^-, 9.64 \text{ MeV})$  and  $^{16}\text{O}(3_1^-, 6.13 \text{ MeV})$  established experimentally. In 1970's, cluster structures of the ground and excited states in  $^{12}\text{C}$  and  $^{16}\text{O}$  have been investigated by using microscopic and semi-microscopic cluster models [3–11], a molecular orbital model [12], and also a hybrid model of shell model and cluster model [13].

For  $^{12}\text{C}$ , the ground state is considered to have the triangle deformation because of the  $3\alpha$ -cluster structure. In addition, a further prominent triangle  $3\alpha$  structure has been suggested in  $^{12}\text{C}(3_1^-, 9.64 \text{ MeV})$ . Although the cluster structure of the ground state,  $^{12}\text{C}(0_1^+)$ , may not be so prominent as that of the  $^{12}\text{C}(3_1^-)$ , the  $J^\pi = 0_1^+$  and  $3_1^-$  states are often described by the rotation of the equilateral triangle  $3\alpha$  configuration having the  $D_{3h}$  symmetry. In contrast to the geometric configuration suggested in  $^{12}\text{C}(0_1^+)$  and  $^{12}\text{C}(3_1^-)$ , a developed  $3\alpha$ -cluster structure with no geometric configuration has been suggested in the  $0_2^+$  state assigned to  $^{12}\text{C}(0_2^+, 7.66 \text{ MeV})$  by (semi-)microscopic three-body calculations of  $\alpha$  clusters [5, 7, 8, 10]. In the  $0_2^+$  state, three  $\alpha$  particles are weakly interacting like a gas, for which the normal concept of nuclear deformation may be no longer valid. For the  $0_2^+$  state, Tohsaki *et al.* has proposed a new interpretation of a dilute cluster gas state, where  $\alpha$  particles behave as bosonic particles and condensate in the  $S$  orbit [14]. This state is now attracting a great interest in relation with the Bose Einstein condensation (BEC) in nuclear matter [15].

Let us consider the cluster phenomena in  $^{12}\text{C}$  from the viewpoint of symmetry breaking. If the symmetry of the rotational invariance is not broken, a nucleus has a spherical shape. In the intrinsic state of  $^{12}\text{C}(0_1^+)$ , the spherical shape changes to the triangle shape via the oblate shape because of the  $\alpha$ -cluster correlation. It is the symmetry breaking from the rotational symmetry to the axial symmetry, and to the  $D_{3h}$  symmetry. In the group theory, it corresponds to  $O(3) \rightarrow O(2) \times Z_2 \rightarrow D_{3h}$ , where the symmetry breaking from the continuous (rotational) group to the discrete (point) group occurs. In the excited state,  $^{12}\text{C}(0_2^+)$ , the system again may have the continuous group  $O(3)$  symmetry. It indicates that the cluster correlations in  $^{12}\text{C}(0_1^+)$  and  $^{12}\text{C}(0_2^+)$  may have different features in terms of symmetry breaking. The triangle shape with the  $D_{3h}$  symmetry in  $^{12}\text{C}(0_1^+)$  is characterized by the geometric configuration, while the  $^{12}\text{C}(0_2^+)$  has no geometric configuration. Now a question arises: what is the mechanism of the symmetry breaking of the continuous group in  $^{12}\text{C}(0_1^+)$ , which is restored again in  $^{12}\text{C}(0_2^+)$ . One of the key problems

is the geometric configuration because of  $\alpha$  correlations in the ground state. The triangle state has oscillating surface density along the oblate edge. It can be understood by the density wave (DW)-like correlation caused by the  $1p$ - $1h$  correlation carrying a finite momentum in analogy to the DW in infinite matter with inhomogeneous periodic densities, which has been an attractive subject in various fields such as nuclear and hadron physics [16–34] as well as condensed matter physics [35, 36]. Indeed, in our previous work, we interpreted the triangle shape as the edge density wave on the oblate state by extending the DW concept to surface density oscillation of finite systems [37]. Then the structures of  $^{12}\text{C}(0_1^+)$  and  $^{12}\text{C}(0_2^+)$  may be associated with the DW and the BEC phases in infinite matter, respectively. The mechanism of the geometric triangle shape in the finite system may give a clue to understand an origin of DW in infinite matter.

Similar to  $^{12}\text{C}$ , a geometric configuration with a tetrahedral shape in  $^{16}\text{O}$  has been discussed in theoretical studies with cluster model calculations [1, 3, 11] and also with Hartree-Fock calculations [38–40]. The excited state,  $^{16}\text{O}(3_1^-, 6.13 \text{ MeV})$ , is understood by the tetrahedron vibration or the rotation of the tetrahedral deformation with the  $T_d$  symmetry, while the static tetrahedral shape in the ground state has not been confirmed yet. The tetrahedron shape in  $^{16}\text{O}(0_1^+)$  and  $^{16}\text{O}(3_1^-)$  is supported in analysis of experimental data such as  $E3$  transition strengths for  $3_1^- \rightarrow 0_1^+$  [41] and  $\alpha$ -transfer cross sections on  $^{12}\text{C}$  [42]. The tetrahedral shape tends to be favored in cluster-model calculations [3, 11]. However, Hartree-Fock calculations with tetrahedral deformed mean-field potentials usually suggest the spherical  $p$ -shell closed state as the lowest solution for  $^{16}\text{O}$  except for the calculations using effective interactions with specially strong exchange forces [38–40]. If the ground state of  $^{16}\text{O}$  has the tetrahedral shape, it may suggest the breaking of the  $O(3)$  symmetry into the  $T_d$  symmetry. In the excited  $0^+$  states of  $^{16}\text{O}$ ,  $^{12}\text{C}+\alpha$  cluster structure was suggested in the  $0_2^+$  state at 6.05 MeV [4, 9, 10, 43, 44]. Moreover, in analogy to the  $3\alpha$ -cluster gas state of  $^{12}\text{C}(0_2^+)$ , a  $4\alpha$ -cluster gas state with the  $\alpha$  condensation feature has been suggested recently in a  $0^+$  state above the  $4\alpha$  threshold [45, 46]. Similarly to  $^{12}\text{C}$ , the possible tetrahedral shape in  $^{16}\text{O}$  may lead to symmetry breaking of the continuous group in  $^{16}\text{O}(0_1^+)$ , which is restored in higher  $0^+$  states. Again, the geometric configuration due to  $\alpha$  correlations in the ground state should be one of the key problems.

Our aim is to clarify the  $\alpha$ -cluster correlations with geometric configurations in the ground states of  $^{12}\text{C}$  and  $^{16}\text{O}$ , and understand the mechanism of the symmetry breaking from continuous (rotational) groups into discrete (point) groups. We first confirm the problem whether the triangle and tetrahedron shapes are favored in the intrinsic states of  $^{12}\text{C}$  and  $^{16}\text{O}$ . For this aim, we use a method of antisymmetrized molecular dynamics (AMD) [47–49] and perform microscopic many-body calculations without assuming existence of any clusters nor geometric configurations. Variation after the spin-parity projections (VAP) is performed in the AMD framework [50]. The AMD+VAP method has been proved to be useful to describe structures of light nuclei. With this method, one of the authors, Y. K-E., has succeeded to reproduce various properties of ground and excited states of  $^{12}\text{C}$  [50, 51], and confirmed the formation and development of three  $\alpha$  clusters in  $^{12}\text{C}$  in the microscopic calculations with no cluster assumptions for the first time. The result was supported also by the work using the method of Fermionic molecular dynamics [52], which shows a similar method to the AMD.

In this paper, we apply the AMD+VAP method to  $^{16}\text{O}$  as well as  $^{12}\text{C}$  and analyze the intrinsic shapes of the ground states. We show that the geometric configurations having the approximate  $D_{3h}$  and  $T_d$  symmetry arise in the ground states of  $^{12}\text{C}$  and  $^{16}\text{O}$ , respectively. To discuss appearance of the geometric configurations, we perform analysis using a simple cluster wave functions of Brink-Bloch (BB)  $\alpha$ -cluster model [53], while focusing on Pauli blocking effect on rotational motion of an  $\alpha$  cluster. Important roles of the Pauli blocking effect in appearance of geometric configurations are described. We also introduce a schematic model by considering clusters on a Fermi gas core in a one-dimensional (1D) finite box, which can be linked with clusters at surface in a  $3\alpha$  system. By analyzing the 1D-cluster wave function, in particular, looking at Pauli blocking effects from the core and those between clusters, we try to conjecture what conditions favor BCS-like, DW-like, and BEC-like correlations.

This paper is organized as follows. In the next section, intrinsic shapes and cluster formation in the ground states of  $^{12}\text{C}$  and  $^{16}\text{O}$  are investigated based on the AMD+VAP calculation. In Sec. III a Pauli blocking effect in  $\alpha$ -cluster systems and its role in  $\alpha$ -cluster correlations is described by analysis of BB  $\alpha$ -cluster wave functions. In Sec. IV, the schematic model of clusters on the Fermi gas core in the 1D finite box is introduced and the roles of Pauli blocking effects in  $\alpha$ -cluster correlations are discussed. Summary and outlook are given in Sec. V. The relations between  $3\alpha$ - and  $4\alpha$ -cluster wave functions and triangle and tetrahedral deformed mean-field wave functions are explained in appendix A. In appendix B and C, features of weak-coupling wave functions in the 1D-cluster model are described.

## II. SHAPES AND CORRELATIONS IN THE GROUND STATES OF $^{12}\text{C}$ AND $^{16}\text{O}$

We discuss here intrinsic deformations of the ground states of  $^{12}\text{C}$  and  $^{16}\text{O}$  based on the AMD+VAP calculation. The AMD method has been applied for various light mass nuclei and has been successful in describing cluster structures as well as shell-model-like structures in light-mass nuclei. In the present work, the AMD+VAP method, i.e., variation

after spin and parity projections in the AMD framework, is applied to  $^{12}\text{C}$  and  $^{16}\text{O}$ . For the details of the framework, the reader is referred to, for instance, Refs. [49, 50].

### A. Variation after projection with AMD wave function

In the AMD framework, we set a model space of wave functions and perform the energy variation to obtain the optimum solution in the model space.

An AMD wave function is given by a Slater determinant of Gaussian wave packets,

$$\Phi_{\text{AMD}}(\mathbf{Z}) = \frac{1}{\sqrt{A!}} \mathcal{A}\{\varphi_1, \varphi_2, \dots, \varphi_A\}, \quad (1)$$

where the  $i$ th single-particle wave function is written by a product of spatial ( $\phi$ ), intrinsic spin ( $\chi^\sigma$ ), and isospin wave functions ( $\chi^\tau$ ) as

$$\varphi_i = \phi_{\mathbf{x}_i} \chi_i^\sigma \chi_i^\tau, \quad (2)$$

$$\phi_{\mathbf{x}_i}(\mathbf{r}_j) = \left(\frac{2\nu}{\pi}\right)^{4/3} \exp\left\{-\nu\left(\mathbf{r}_j - \frac{\mathbf{X}_i}{\sqrt{\nu}}\right)^2\right\}, \quad (3)$$

$$\chi_i^\sigma = \left(\frac{1}{2} + \xi_i\right)\chi_\uparrow + \left(\frac{1}{2} - \xi_i\right)\chi_\downarrow. \quad (4)$$

$\phi_{\mathbf{x}_i}$  and  $\chi_i^\sigma$  are spatial and spin functions, and  $\chi_i^\tau$  is the isospin function fixed to be up (proton) or down (neutron). Accordingly, an AMD wave function is expressed by a set of variational parameters,  $\mathbf{Z} \equiv \{\mathbf{X}_1, \mathbf{X}_2, \dots, \mathbf{X}_A, \xi_1, \xi_2, \dots, \xi_A\}$ . The width parameter  $\nu$  relates to the size parameter  $b$  as  $\nu = 1/2b^2$  and it is chosen to be  $\nu = 0.19 \text{ fm}^{-2}$  that minimizes energies of  $^{12}\text{C}$  and  $^{16}\text{O}$ .

The center positions  $\mathbf{X}_1, \mathbf{X}_2, \dots, \mathbf{X}_A$  of single-nucleon wave packets are independently treated as variational parameters. Thus existence of any clusters are not *a priori* assumed in the AMD framework. Despite of it, the model wave function can describe shell-model structures and cluster structures because of the antisymmetrizer and the flexibility of spatial configurations of Gaussian centers. If a cluster structure is favored in a system, the corresponding cluster structure is automatically obtained in the energy variation.

For even-even nuclei, the ground states are known to be  $J^\pi = 0^+$  states, i.e., they are symmetric for rotation. Intrinsic deformation is understood as spontaneous symmetry breaking with respect to the rotational invariance, which is restored in the  $J^\pi = 0^+$  ground states. It means that when an intrinsic state has a deformation the ground state is constructed by the spin and parity projections from the intrinsic state. In more general, spin and parity are good quanta in energy eigenstates of nuclei because of the invariance of the Hamiltonian for rotation and parity transformation. Therefore, to express a  $J^\pi$  state, an AMD wave function is projected onto the spin-parity eigenstate,

$$\Phi(\mathbf{Z}) = P_{MK}^{J\pi} \Phi_{\text{AMD}}(\mathbf{Z}), \quad (5)$$

where  $P_{MK}^{J\pi}$  is the spin-parity projection operator.

To obtain the wave function for a  $J^\pi$  state, the energy variation is performed for the spin-parity projected AMD wave function  $\Phi(\mathbf{Z})$  with respect to variational parameters  $\{\mathbf{Z}\}$ . This method is called variation after projection (VAP). The AMD+VAP method has been applied to various light nuclei for structure study of ground and excited states. For the ground states of  $^{12}\text{C}$  and  $^{16}\text{O}$ , we perform the variation of the energy expectation value  $\langle \Phi(\mathbf{Z}) | H | \Phi(\mathbf{Z}) \rangle / \langle \Phi(\mathbf{Z}) | \Phi(\mathbf{Z}) \rangle$  for the  $J^\pi = 0^+$  projected wave function and get the optimum parameter set  $\{\mathbf{Z}\}$  that minimizes the energy. Then, the AMD wave function  $\Phi_{\text{AMD}}(\mathbf{Z})$  given by the optimized  $\{\mathbf{Z}\}$  is regarded as the intrinsic wave functions of the ground state.

An AMD wave function is expressed by a single Slater determinant; however, the spin-parity projected wave function is no longer a Slater determinant but it is a linear combination of Slater determinants except for the case that the AMD wave function before the projection is already a spin-parity  $J^\pi$  eigenstate. If the intrinsic state has a deformation the projected wave function contains some kinds of correlations beyond Hartree-Fock approximation.

### B. Intrinsic structures of $^{12}\text{C}$ and $^{16}\text{O}$

We apply the AMD+VAP method to the ground states of  $^{12}\text{C}$  and  $^{16}\text{O}$ , and discuss their intrinsic structures.

### 1. Density distribution

The ground states of  $^{12}\text{C}$  and  $^{16}\text{O}$  have the intrinsic deformations. The density distribution of the intrinsic wave functions  $\Phi_{\text{AMD}}$  are shown in Fig. 1. The result for  $^{12}\text{C}$  shows a triaxial deformation with a triangle feature, while  $^{16}\text{O}$  has a deformation with a tetrahedral feature. The quadrupole deformation parameters  $(\beta, \gamma)$  evaluated by the quadrupole moments are  $(\beta, \gamma) = (0.31, 0.13)$  for  $^{12}\text{C}$  and  $(\beta, \gamma) = (0.25, 0.09)$  for  $^{16}\text{O}$ . The triangle and tetrahedral shapes are caused by  $\alpha$ -cluster correlations. Strictly speaking  $\alpha$  clusters are not ideal  $(0s)^4$  clusters but somewhat dissociated ones. Moreover, the triangle and tetrahedron are not regular but distorted as an  $\alpha$  cluster is situated slightly far from the other  $\alpha$ s.

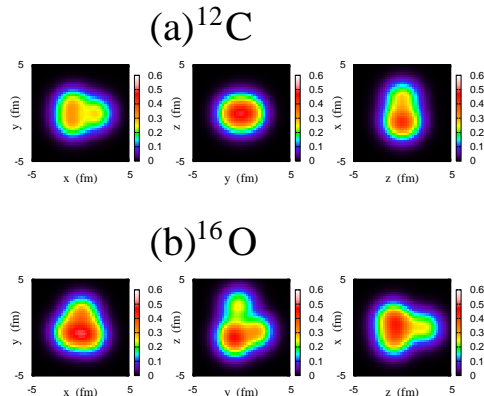


FIG. 1: (color on-line) Density distributions in the intrinsic states for the ground states of (top)  $^{12}\text{C}$  and (bottom)  $^{16}\text{O}$  obtained by the AMD+VAP calculation. The density integrated on the  $z$ ,  $x$ , and  $y$  axes is plotted on the  $x$ - $y$ ,  $y$ - $z$ , and  $z$ - $x$  planes.

### 2. Oscillation of the surface density

Let us consider the deformations of  $^{12}\text{C}$  and  $^{16}\text{O}$  from the viewpoint of symmetry breaking. The highest symmetry is the sphere, which is realized in the closed  $p^{3/2}$ -shell and  $p$ -shell states for  $^{12}\text{C}$  and  $^{16}\text{O}$ , respectively. As a higher symmetry can break into lower symmetry due to multi-nucleon correlations, the deformation mechanism of  $^{12}\text{C}$  is interpreted as follows. Because of the  $\alpha$ -cluster correlations, the rotational symmetry in the sphere breaks to the axial symmetry in an oblate deformation and changes into the  $D_{3h}$  symmetry in the regular triangle  $3\alpha$  configuration, and then it breaks to the distorted triangle. The symmetry change, spherical $\rightarrow$ oblate $\rightarrow$ triangle, corresponds to  $O(3) \rightarrow O(2) \times Z_2 \rightarrow D_{3h}$ . Similarly, the deformation of  $^{16}\text{O}$  is understood as the rotational symmetry in the sphere breaks into the  $T_d$  symmetry in the regular tetrahedral  $4\alpha$  configuration, and it breaks to the distorted tetrahedron. The structure change from the spherical to the tetrahedron is the breaking of the  $O(3)$  symmetry to the  $T_d$  symmetry. Note that the continuous (rotational) groups break to the discrete (point) groups in the triangle and tetrahedron deformations.

We discuss the connection of cluster correlations with the density wave, which is characterized by the static density oscillation at the surface. The surface density oscillation occurs at the symmetry breaking from the axial symmetry (oblate shape) to the  $D_{3h}$  symmetry (triangle) in  $^{12}\text{C}$  and that from the rotational symmetry (sphere) to the  $T_d$  symmetry (tetrahedron) in  $^{16}\text{O}$ . The triangle deformation contains the  $(Y_3^{-3} - Y_3^{+3})/\sqrt{2}$  component with the  $Y_2^0$  deformation in the density, while the tetrahedral one has the  $(\sqrt{5}Y_3^0 + \sqrt{2}Y_3^{-3} - \sqrt{2}Y_3^{+3})/3$  component, which can be transformed to  $(Y_3^{-2} + Y_3^{+2})/\sqrt{2}$  by the rotation. Indeed, as described in appendix A, an ideal  $3\alpha(4\alpha)$ -cluster wave function with the triangle (tetrahedral) configuration has the density having the finite components of  $(Y_3^{-3} - Y_3^{+3})/\sqrt{2}$  ( $(\sqrt{5}Y_3^0 + \sqrt{2}Y_3^{-3} - \sqrt{2}Y_3^{+3})/3$ ) and it can be described by the DW-type particle-hole correlations in case of weak deformations. Note that the DW in the triangle shape is characterized by the particle-hole correlations on the Fermi surface carrying the finite angular momentum  $(l, m) = (3, \pm 3)$  and that in the tetrahedral one is given by the particle-hole correlations with  $(l, m) = (3, \pm 2)$  as described in the appendix. Namely, the symmetry breaking is characterized by the  $(Y_3^{-3} - Y_3^{+3})/\sqrt{2}$  component whose amplitudes linearly relate to the order parameter of the DW correlations as shown in Eqs. (A3), (A6), and (A7). In other words, the symmetry broken states have finite  $(Y_3^{-3} - Y_3^{+3})/\sqrt{2}$  components in surface density and show the oscillation density with the wave number three.

To analyze the surface density oscillation in the ground states of  $^{12}\text{C}$  and  $^{16}\text{O}$ , we perform the multipole decomposition of the intrinsic density obtained with the AMD+VAP calculation

$$\rho(r = R_0, \theta, \phi) = \bar{\rho}(R_0) \sum_{lm} \alpha_{lm} Y_l^m(\theta, \phi), \quad (6)$$

at a certain radius  $r = R_0$ , and discuss the  $(Y_3^{-3} - Y_3^{+3})/\sqrt{2}$  components. We take  $R_0$  to be the root mean square radius of the intrinsic state.  $\bar{\rho}(R_0)$  is determined by the normalization  $\alpha_{00} = 1$ , and  $\alpha_{lm}$  has the relation  $\alpha_{lm} = (-1)^m \alpha_{l-m}^*$  because the density  $\rho(r = R_0, \theta, \phi)$  is real.

The density plot at  $r = R_0$  on the  $\theta$ - $\phi$  plane for  $^{12}\text{C}$  and that at  $r = R_0$  and  $\theta = \pi/2$  as a function of  $\phi$  are shown in Fig. 2. As seen clearly, the density on the oblate edge shows the oscillation with the approximate wave number three periodicity, which comes from the  $\alpha$ -cluster correlation. In the right panel of Fig. 2, we also plot the density for the ideal  $D_{3h}$  symmetry given only by the  $(l, m) = (0, 0), (2, 0), (3, 3)$  and  $(3, -3)$  components to show somewhat distortion of the AMD+VAP result from the ideal  $D_{3h}$  symmetry. In the coefficients  $|\alpha_{lm}|$  shown in Fig. 4, it is found that the  $Y_l^{\pm 3}$  components are actually finite indicating that the axial symmetry is broken to the triangle shape in  $^{12}\text{C}$ .

For the density in  $^{16}\text{O}$ , the  $\theta$ - $\phi$  plot is shown in Fig. 3, and the coefficients of the multipole decomposition are shown in Fig. 4. The tetrahedral component  $\sqrt{5}Y_3^0/3 + \sqrt{2}Y_3^{+3}/3 - \sqrt{2}Y_3^{-3}/3$  is shown by the hatched boxes at  $\alpha_{30}$  and  $\alpha_{33}$  in Fig. 4. The open boxes indicate the distortion components from the tetrahedron. The distortion exists in the axial symmetry components,  $\alpha_{30}$ ,  $\alpha_{20}$ , and  $\alpha_{10}$ , coming from the spatial development of an  $\alpha$  cluster from the others as explained before.

Thus, the intrinsic states of  $^{12}\text{C}$  and  $^{16}\text{O}$  show the surface density oscillation with the  $(Y_3^{-3} - Y_3^{+3})/\sqrt{2}$  component. The wave number three oscillation characterized by the  $(Y_3^{-3} - Y_3^{+3})/\sqrt{2}$  component is understood by the  $\alpha$ -cluster correlations with triangle and tetrahedral deformations, which are interpreted as the DWs on the oblate and spherical shapes, i.e., the spontaneous symmetry breaking of axial symmetry  $\rightarrow D_{3h}$  and rotational symmetry  $\rightarrow T_d$  symmetry.

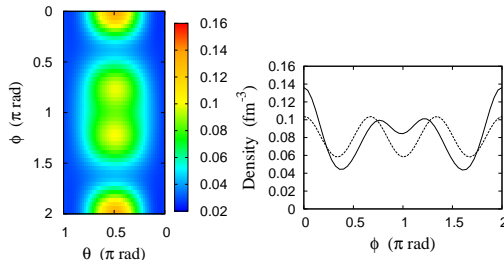


FIG. 2: (color on-line) Left: density at  $r = R_0$  for  $^{12}\text{C}$  calculated by the AMD+VAP is plotted on the  $\theta$ - $\phi$  plane. Right: that at  $r = R_0$  and  $\theta = \pi/2$  line (the solid line). The density for the ideal  $D_{3h}$  symmetry given only by the  $(l, m) = (0, 0), (2, 0), (3, 3)$  and  $(3, -3)$  components is also plotted (the dashed line).  $R_0$  is taken to be 2.53 fm.

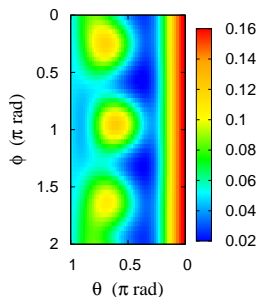


FIG. 3: (color on-line) density at  $r = R_0$  for  $^{16}\text{C}$  calculated by the AMD+VAP is plotted on the  $\theta$ - $\phi$  plane.  $R_0$  is chosen to be 2.81 fm.

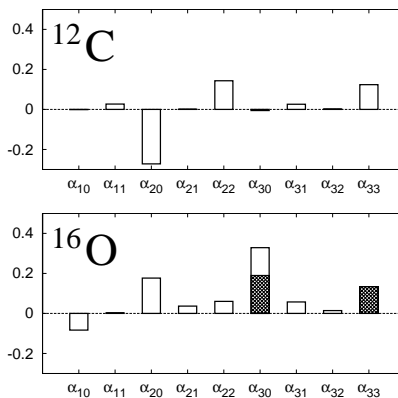


FIG. 4: The coefficients  $\alpha_{lm}$  of the multipole decomposition of the intrinsic density of (top)  $^{12}\text{C}$  and (bottom)  $^{16}\text{O}$  calculated by the AMD+VAP. The hatched areas in the bottom panel are the tetrahedron component  $\sqrt{5}Y_3^0/3 + \sqrt{2}Y_3^{+3}/3 - \sqrt{2}Y_3^{-3}/3$  defined by  $\alpha_{30}^{\text{hatch}} \equiv \sqrt{5/2}\alpha_{33}$  and  $\alpha_{33}^{\text{hatch}} \equiv \alpha_{33}$ . The open area for the  $Y_3^0$  component is defined by the relation  $\alpha_{30} = \alpha_{30}^{\text{open}} + \alpha_{30}^{\text{hatch}}$ .

### III. PAULI BLOCKING EFFECT IN $\alpha$ CORRELATIONS

As shown in the previous section, the intrinsic states of  $^{12}\text{C}$  and  $^{16}\text{O}$  obtained with the AMD+VAP calculation contain the  $\alpha$ -cluster correlations with the triangle and tetrahedral deformations. For  $^{12}\text{C}$ , the triangle deformation has been suggested in  $3\alpha$ -cluster models, in which  $3\alpha$  state with a regular triangle configuration is the energy minimum state [3, 7, 10]. In contrast to such the geometric configuration as the triangle, the second  $0^+$  state of  $^{12}\text{C}$  is considered to be a cluster gas state where 3  $\alpha$  clusters are freely moving in dilute density like a gas without any geometric correlations between clusters [7, 8, 10, 14]. The  $0_2^+$  state is associated with the  $\alpha$  condensation in analogy to BEC because it is regarded as a system of three  $\alpha$ s occupying the same  $S$  orbit [14].

From the viewpoint of symmetry breaking, the symmetry is broken in the  $0_1^+$  state with the triangle deformation and it is restored in the  $0_2^+$  state. In the  $0_1^+$  state, the axial symmetry breaks down to the  $D_{3h}$  symmetry due to the  $3\alpha$ -cluster structure. One of the characteristics of the  $0_1^+$  state is the oscillating surface density caused by the angular correlation of  $\alpha$  clusters. Then the structure change from the  $0_1^+$  to the  $0_2^+$  is expected to connect with the transition from the symmetry broken state with the angular correlation to the symmetric state with no (or less) correlation between  $\alpha$  clusters.

The origin of the angular correlation in the  $0_1^+$  state and the transition into the uncorrelated  $0_2^+$  state can be understood by the Pauli blocking effect between clusters as follows. Let us here consider motion of an  $\alpha$  cluster around a  $2\alpha$  core in the BB  $3\alpha$ -cluster model wave function. In the BB  $3\alpha$ -cluster model,  $\alpha$  clusters are located around certain positions  $\mathbf{S}_1$ ,  $\mathbf{S}_2$ , and  $\mathbf{S}_3$ , and the wave function is written as

$$\Phi_{BB}(\mathbf{S}_1, \mathbf{S}_2, \mathbf{S}_3) = \frac{1}{\sqrt{A!}} \mathcal{A} \{ \Pi_{\tau\sigma} \phi_{\mathbf{S}_1} \mathcal{X}_{\tau\sigma} \phi_{\mathbf{S}_2} \mathcal{X}_{\tau\sigma} \phi_{\mathbf{S}_3} \mathcal{X}_{\tau\sigma} \}, \quad (7)$$

where  $\mathcal{X}_{\tau\sigma}$  is the spin-isospin wave function with  $\tau = \{p, n\}$  and  $\sigma = \{\uparrow, \downarrow\}$ . We assume that 2  $\alpha$  clusters placed at  $\mathbf{S}_1 = (0, 0, d/2)$  and  $\mathbf{S}_2 = (0, 0, -d/2)$  form the core. The third  $\alpha$  is placed at  $\mathbf{S}_3 = (0, y, z)$  for  $y = r \cos \theta_y$ ,  $z = r \sin \theta_y$  on the  $(y, z)$ -plane (see Fig. 5). Because of Pauli blocking effect between clusters, the motion of the third  $\alpha$  around the core is restricted in the Pauli allowed region. Particularly when the  $\alpha$  exists near the core, rotational motion is strongly blocked because of the existence of other  $\alpha$  clusters. The Pauli allowed and forbidden areas for the rotation of the angle  $\theta_y$  for the third  $\alpha$  center in the  $(y, z)$ -plane are presented in Fig. 5. In the figure, the norm  $\mathcal{N}_{3\alpha}(y, z) = \langle \Phi_{BB}(\mathbf{S}_1, \mathbf{S}_2, \mathbf{S}_3) | \Phi_{BB}(\mathbf{S}_1, \mathbf{S}_2, \mathbf{S}_3) \rangle$  of the BB wave function  $\Phi_{BB}(\mathbf{S}_1, \mathbf{S}_2, \mathbf{S}_3)$  with the parameters,  $\mathbf{S}_1 = (0, 0, d/2)$ ,  $\mathbf{S}_2 = (0, 0, -d/2)$ , and  $\mathbf{S}_3 = (0, y, z)$  is shown in the  $(y, z)$ -plane.  $d$  is fixed and taken to be a small value. The norm is normalized by the value for the  $\alpha$  on the  $y$ -axis,

$$\tilde{\mathcal{N}}_{3\alpha}(y, z) \equiv \frac{\mathcal{N}_{3\alpha}(y = r \cos \theta_y, z = r \sin \theta_y)}{\mathcal{N}_{3\alpha}(y = r, z = 0)}. \quad (8)$$

The area with  $\tilde{\mathcal{N}}_{3\alpha} \sim 1$  is the allowed region where the  $\alpha$  feels no Pauli blocking with respect to the rotational motion, while the  $\tilde{\mathcal{N}}_{3\alpha} \sim 0$  region is the blocked region where it feels the strong Pauli blocking effect from  $\alpha$  clusters of the core. It means that, when the third  $\alpha$  exists near the core, its angular motion is blocked by the  $2\alpha$  core. As a result, the third  $\alpha$  is confined in the Pauli allowed region around the  $y$  axis, and it has the angular correlation

against the  $2\alpha$  direction. Consequently, a compact  $3\alpha$  state has a geometric structure of the triangle deformation and it has the surface density oscillation. On the other hand, as the cluster develops specially the Pauli blocking effect becomes weak. When the  $\alpha$  is far enough from the core, it can freely move in the rotational mode. Then the angular correlation vanishes and the system transits to angular-uncorrelated state. We note that in cluster physics this transition is known to be the change between strong cluster coupling and weak cluster coupling states, where the angular momentum of the inter-cluster motion couples with inner spins of clusters strongly and weakly, respectively (see Fig. 5). What we call the cluster coupling is coupling between clusters and it is different from the terminology of strong and weak couplings in the BEC-BCS crossover phenomena, which relate to the coupling between nucleons in a pair (or in a cluster).

The  $0_1^+$  state of  $^{12}\text{C}$  is considered to be the compact  $3\alpha$  state in the strong Pauli blocking regime and corresponds to the angular correlated state with the surface density oscillation due to the triangle deformation. In the  $^{12}\text{C}(0_2^+)$ , clusters spatially develop well and the system goes to the non-angular-correlation state. Strictly speaking, in the  $^{12}\text{C}(0_2^+)$ , all clusters develop to form an uncorrelating three  $\alpha$  state associated with the  $\alpha$  condensation, where the radial motion is also important as well as the angular motion. Nevertheless, we can say that, for the restoration of the broken symmetry with the surface density oscillation in the  $0_1^+$  to the rotational symmetry in the  $0_2^+$ , the transition from the angular correlated state to the uncorrelated state in the cluster development is essential.

In the above discussion, we consider the angular motion in the intrinsic (body-fixed) frame, i.e., the  $y$ - $z$  plane. Since the system is symmetric for the rotation around the  $z$ -axis, the motion of the third  $\alpha$  is free for the  $z$ -rotation. This rotational mode around the  $z$  axis is nothing but the projection onto the  $J_z = 0$ , which is usually performed in the  $J^\pi = 0^+$  projection of the intrinsic state.

Also in  $^{16}\text{O}$ , the angular motion of an  $\alpha$  cluster at the surface is blocked by other three  $\alpha$ s. The Pauli blocking effect between  $\alpha$  clusters causes the angular correlation of the tetrahedral configurations in a compact  $4\alpha$  state. For transition from the angular correlated cluster state of the ground state to the uncorrelated cluster state like a cluster gas, at least two  $\alpha$  clusters need to spatially develop to move freely in the allowed region without feeling the Pauli blocking effect. The  $4\alpha$ -cluster gas state in  $^{16}\text{O}$  has been suggested near the  $4\alpha$  threshold energy. The suggested excitation energy  $E_x \sim 15$  MeV is almost twice of  $E_x = 7.66$  MeV for the  $3\alpha$ -cluster gas state in  $^{12}\text{C}$ . This might correspond to the energy cost of the spatial development for two  $\alpha$ s in  $^{16}\text{O}$  compared with that for an  $\alpha$  in  $^{12}\text{C}$ .

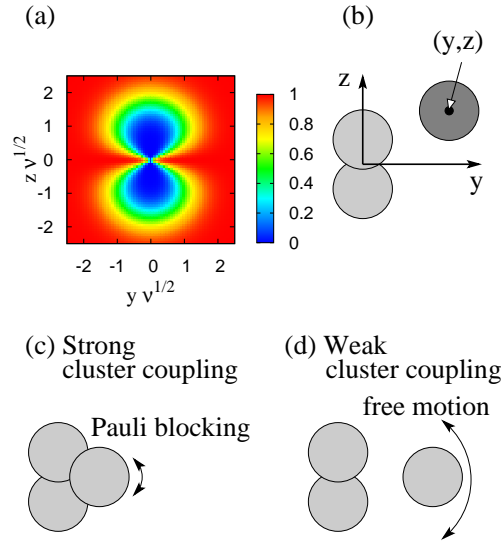


FIG. 5: (a) The Pauli allowed and forbidden regions for the rotation of the angle  $\theta_y$  for the third  $\alpha$  in the  $(y, z)$ -plane around the  $2\alpha$  core. The norm  $\tilde{N}_{3\alpha}(y = r \cos \theta_y, z = r \sin \theta_y)$  normalized at  $(y = 0, z = r)$  is presented. The  $\tilde{N}_{3\alpha} \sim 1$  and  $\tilde{N}_{3\alpha} \sim 0$  regions are the Pauli allowed and forbidden regions, respectively. (b) A schematic figure for the position of the third  $\alpha$  around the  $2\alpha$  core. (c) A schematic figure of the strong cluster coupling state for a compact  $3\alpha$  state with the strong the Pauli blocking effect, and (d) that of the weak cluster coupling state. See the text.

## IV. CLUSTERS ON A FERMI GAS CORE IN ONE DIMENSIONAL BOX

### A. Concept of one-dimensional cluster model

As mentioned, the triangle deformation of the  $^{12}\text{C}$  ground state can be interpreted as the density wave on the axial symmetric oblate state and it is characterized by the static surface density oscillation with the wave number three on the edge of the oblate intrinsic state. The symmetry breaking in the ground state originates in the 4-body correlation in  $\alpha$  clusters. The axial symmetry is broken by the angular correlation between  $\alpha$  clusters due to the Pauli blocking effect. As  $\alpha$  clusters develop, the Pauli blocking weakens and the angular correlation vanishes. Then the system transits from the symmetry broken state of the  $^{12}\text{C}(0_1^+)$  to the symmetry restored state of the  $^{12}\text{C}(0_2^+)$ , where  $\alpha$  clusters are freely moving in a dilute density like a gas.

In this section, we consider Pauli blocking effects in a schematic model of two clusters on a Fermi gas core in a one-dimensional (1D) finite box, and discuss how the translational invariance is broken to form an oscillating density (inhomogeneous) state and how the broken symmetry is restored to a uniform density (homogeneous) state.

Let us consider a schematic model for a simplified  $3\alpha$  system consisting of two  $\alpha$  clusters around the  $\alpha$  core. To concentrate only on angular correlations between two  $\alpha$ s, we ignore the radial coordinate degree of freedom and assume that two  $\alpha$  clusters are moving at a certain distance  $r_0$  from the core. Taking the body-fixed frame so as one of two  $\alpha$  clusters on the  $z$ -axis and the other  $\alpha$  in the  $y$ - $z$  plane, then, the angular motion between two  $\alpha$ s can be reduced to the 1D problem, where the first cluster sits around the origin and the second cluster exists in a finite size  $L = 2\pi r_0$  box with the periodic boundary condition. For the core effect, we take into account only the Pauli blocking from the core particles, which is treated here by a Fermi gas core for simplicity.

We extend the 1D-cluster model and treat the cluster size  $b$ , the box size  $L$ , and the core Fermi momentum  $k_c$  as parameters. In this model, we do not perform energy variation nor calculate energy eigenstates. Moreover, the mechanism of cluster formation and the dynamical change of the cluster structure or the cluster size are beyond our scope. We give a model wave function with fixed parameters  $b, L, k_c$  based on simple ansatz, and analyze Pauli blocking effect between a cluster and the core and that between two clusters in the given wave function. From behavior of the wave function and features of the Pauli blocking effects, we conjecture how the transition between the Fermi gas, BCS-like, DW-like, and BEC-like states occurs.

### B. Formulation of one-dimensional cluster model

We explain details of the 1D-cluster model wave function. Two  $n$ -body clusters are formed on a Fermi gas core in a 1D box with the box size  $L = 2\pi r_0$ . For an  $\alpha$  cluster  $n = 4$  and a cluster consists of  $p \uparrow, p \downarrow, n \uparrow,$  and  $n \downarrow$ . Basis single-particle wave functions in the periodic boundary condition are given as  $e^{+ikx}/\sqrt{2L}$  and  $e^{-ikx}/\sqrt{2L}$ , where the momentum  $k = 2\pi\tilde{k}/L$ . Here  $\tilde{k}$  is the dimensionless momentum  $\tilde{k} = kr_0$  and takes  $\tilde{k} = 0, 1, 2, 3, \dots$ . Core nucleons are assumed to form a Fermi surface at  $k_c$ . It means that  $k \leq k_c$  orbits are occupied by core nucleons and they are forbidden single-particle states for constituent nucleons of clusters. Using the dimensionless parameter  $\tilde{k}_c = k_c r_0$ , the lowest allowed momentum is  $k_F = \tilde{k}_F/r_0$  for  $\tilde{k}_F \equiv \tilde{k}_c + 1$  and  $k \geq k_F$  orbits are allowed.

We assume the first cluster ( $\alpha_1$ ) wave function that localized around  $x = 0$  in a Gaussian form,

$$\psi_{\alpha_1} = \Pi_{\chi} \phi_0(x_{1\chi}) \mathcal{X}_{\chi}, \quad (9)$$

$$\chi = \tau\sigma = \{p \uparrow, p \downarrow, n \uparrow, n \downarrow\}, \quad (10)$$

$$\phi_0(x) = \frac{1}{\sqrt{2L}} \sum_{k \geq k_F} f(k) (e^{+ikx} + e^{-ikx}). \quad (11)$$

$f(k)$  is the Fourier transformation of the Gaussian with the cluster size  $b$  and given as

$$f(k) = n_0 \exp\left(-\frac{b^2 k^2}{2}\right), \quad (12)$$

where  $n_0$  is determined by the condition,

$$\sum_{k \geq k_F} |f(k)|^2 = 1, \quad (13)$$

to normalize  $\phi_0(x)$  in the box. The wave function indicates that four species of nucleons,  $p \uparrow, p \downarrow, n \uparrow, n \downarrow$ , occupy the same spatial orbit with the Gaussian form forbidden partially by the Fermi gas core. If  $b/L$  and  $k_F$  are small enough,

the wave function is localized well around  $x = 0$ . Since there is no identical Fermion in a cluster, the antisymmetrizer can be omitted in the expression.

Next we consider the second cluster ( $\alpha_2$ ). Assuming that  $\alpha_2$  is localized around a position  $x = s$ , the wave function is given by the shifted function,

$$\psi_{\alpha_2}^s = \prod_{\sigma} \phi_s(x_{2\chi}) \mathcal{X}_{\chi}, \quad (14)$$

$$\phi_s(x) = \frac{1}{\sqrt{2L}} \sum_{k \geq k_F} f(k) \left( e^{+ik(x-s)} + e^{-ik(x-s)} \right). \quad (15)$$

Then, the normalized wave function of the  $2\alpha$  system with the parameter  $s$  is written as

$$\Psi_s = \mathcal{N}_{\text{PB}}^{-2}(s) \frac{1}{8!} \mathcal{A} \{ \psi_{\alpha_1} \psi_{\alpha_2}^s \}, \quad (16)$$

$$\mathcal{N}_{\text{PB}}(s) \equiv \left| \frac{1}{\sqrt{2}} \mathcal{A} \{ \phi_0 \phi_s \} \right|^2 \quad (17)$$

$$= \frac{1}{2} |\phi_0(x_1) \phi_s(x_2) - \phi_0(x_2) \phi_s(x_1)|^2 \quad (18)$$

$$= 1 - \langle \phi_0 \phi_s | \phi_s \phi_0 \rangle. \quad (19)$$

$\mathcal{N}_{\text{PB}}(s)$  is the overlap norm for two identical nucleons. It is a function of the parameter  $s$  for the localization center of the second cluster.  $\mathcal{N}_{\text{PB}}^4$  means the overlap norm for the  $2\alpha$  system and it is an indicator to evaluate the Pauli blocking effect between two clusters. In the case that two clusters feel no Pauli blocking,  $\mathcal{N}_{\text{PB}}^4(s) = 1$ , while in the case that they feel complete Pauli blocking,  $\mathcal{N}_{\text{PB}}^4 = 0$ . It means that  $\mathcal{N}_{\text{PB}}^4(s)$  stands for the Pauli "allowedness" for  $\alpha_2$  around  $s$ .

The density distribution for  $\chi = \tau\sigma$  particles in the  $2\alpha$  state is

$$\rho_s^{\chi}(x) = \langle \Psi_s | \sum_{i \in \chi} \delta(x - x_i) | \Psi_s \rangle. \quad (20)$$

Note that the density distributions for all kinds of nucleons are the same in the present cluster model and the total nuclear density is  $\sum_{\chi} \rho_s^{\chi}(x) = 4\rho_s^{\chi}(x)$ . In a similar way, the  $\chi = \tau\sigma$  density for the one- $\alpha$  state  $\psi_{\alpha_1}$  is

$$\rho_{\alpha_1}^{\chi}(x) = \langle \psi_{\alpha_1} | \sum_{i \in \chi} \delta(x - x_i) | \psi_{\alpha_1} \rangle. \quad (21)$$

In the present model, we can express all the formulation with the dimensionless parameters  $\tilde{L} = L/r_0 = 2\pi$ ,  $\tilde{b} = b/r_0$ ,  $\tilde{s} = s/r_0$ ,  $\tilde{x} = x/r_0$ ,  $\tilde{k} = kr_0$ ,  $\tilde{k}_c = k_c r_0$ ,  $\tilde{k}_F = k_F r_0$ , and so on. The dimensionless densities are also defined as  $\tilde{\rho} = \rho r_0$ . Then, the state  $|\Psi_s\rangle$  is specified with the dimensionless parameters  $(\tilde{k}_F, \tilde{b}, \tilde{s})$  and does not depend on the scaling factor  $r_0$ . Since the number of clusters is fixed to be two, a larger volume size  $L$  corresponds to a lower cluster density. Because of the scaling, a larger volume size  $L = 2\pi r_0$  with a fixed cluster size  $b$  is equivalent to a smaller cluster size  $b$  with a fixed  $L$ . That means, the parameter  $\tilde{b}$  indicates the cluster size relative to the box size and also corresponds to the cluster density. The  $\tilde{k}_F = \tilde{k}_c + 1$  is the lowest allowed momentum just above the core Fermi momentum  $\tilde{k}_c$ , and it relates to the density of the core particles.

### C. Pauli blocking effect from the core to one cluster

Let us describe the structure change of one cluster on the Fermi gas core in the 1D-cluster model. The coefficients  $f(\tilde{k})$  of the Fourier transformation and the density distribution  $\rho_{\alpha_1}^{\chi}(\tilde{x})$  for the  $\alpha_1$  cluster are shown in Figs. 6 and 7 for  $\tilde{k}_F = 1$  and  $\tilde{k}_F = 2$ , respectively. Because of the Pauli blocking effect from the core as well as the finite volume effect, the structure of the cluster changes from the original Gaussian form depending of the parameters  $\tilde{b}$  and  $\tilde{k}_F$ . In the case of small  $\tilde{b}$ , which corresponds to the small cluster size  $b$  or the large volume size  $L$ , the coefficient  $f(\tilde{k})$  is distributed widely and has a long tail toward the high momentum region, and the density is localized well around  $\tilde{x} = 0$  (and also  $\tilde{x} = 2\pi$  for the periodic boundary). With increase of  $\tilde{k}_F$ , the low momentum components are truncated and the density shows a oscillating tail. Nevertheless, if the cluster size  $\tilde{b}$  is small enough, the density is still localized. With increase of the cluster size  $\tilde{b}$ , the density localization weakens and the density approaches the periodic one. Then,

the component of the lowest allowed orbit  $\tilde{k}_F = \tilde{k}_c + 1$  is dominant and the components of higher orbits decrease. The localization declines more rapidly in the case of the larger  $\tilde{k}_F$ . It means that, as the  $\tilde{b}$  increases or as the  $\tilde{k}_F$  increases, the spatial correlation between nucleons (inner correlation) in a cluster becomes weak. We call the case of the weak localization that the wave function has the dominant  $\tilde{k}_F$  component and minor  $\tilde{k} > \tilde{k}_F$  components “the weak coupling regime”, and the opposite case of the strong localization with significant  $\tilde{k} > \tilde{k}_F$  components “the strong coupling regime”. In the weak coupling limit, the one-cluster density goes to  $\cos^2(\tilde{k}_F \tilde{x})/\pi$ .

#### D. Pauli blocking between two clusters

For two  $\alpha$  clusters expressed by the cluster wave function  $\Psi_s$ , the clusters  $\alpha_1$  and  $\alpha_2$  are assumed to be localized around  $\tilde{x} = 0$  and  $\tilde{x} = \tilde{s}$ , respectively. The Pauli blocking effect between  $\alpha_1$  and  $\alpha_2$  is evaluated by the overlap norm  $\mathcal{N}_{\text{PB}}^4(\tilde{s})$ , which is an indicator for Pauli allowedness. The Pauli allowedness  $\mathcal{N}_{\text{PB}}^4(\tilde{s}) \sim 0$  means that the  $\tilde{s}$  region is blocked by the  $\alpha_1$  cluster and is a forbidden area for  $\alpha_2$ . The middle panels of Figs. 6 and 7 show the allowedness  $\mathcal{N}_{\text{PB}}^4(\tilde{s})$  (thin solid lines) as well as  $\mathcal{N}_{\text{PB}}(\tilde{s})$  (dashed lines) plotted as a function of  $\tilde{s}$ . In principle, the Pauli blocking effect reflects the probability of the  $\alpha_1$  cluster, and therefore, the forbidden region corresponds to the relatively high density region of the  $\alpha_1$  cluster. In case of a small cluster size  $\tilde{b}$ , the allowed region exists widely and the forbidden region exists only in the small area close to  $\tilde{x} = 0$  and  $\tilde{x} = 2\pi$ . That is to say, the second cluster feels almost no Pauli blocking effect except for the region near the first cluster ( $\alpha_1$ ). With increase of  $\tilde{b}$ , the forbidden area spreads in a wide region around  $\tilde{x} = 0$  and  $\tilde{x} = 2\pi$ , and the allowed region for  $\alpha_2$  becomes narrow. In the weak coupling regime, where the  $\alpha_1$  density is periodic, the allowed region with  $\mathcal{N}_{\text{PB}}^4(\tilde{s}) \sim 1$  also shows the periodicity. Reflecting the  $\cos^2(\tilde{k}_F x)$  periodicity of  $\rho_{\alpha_1}(x)$ , the areas  $\tilde{s} \approx \pi 2m/2\tilde{k}_F$  ( $m = 0, \dots, 2\tilde{k}_F$ ) are the forbidden regions, while the areas  $\tilde{s} = \tilde{s}_j = \pi(2j - 1)/2\tilde{k}_F$  ( $j = 1, \dots, 2\tilde{k}_F$ ) are the allowed regions.

As mentioned, the parameter  $\tilde{b}$  corresponds to the cluster size relative to the box size. When the cluster density is low enough, the Pauli blocking effect is weak and almost all region is allowed for the  $\alpha_2$  cluster except for the position close to the  $\alpha_1$ . On the other hand, in the case of the high cluster density the Pauli blocking effect is strong and the allowed  $s$  region is restricted in the periodic regions.

#### E. Transitions from strong coupling to weak coupling regimes

We first discuss the features of the two cluster wave function  $\Psi_s$  with a fixed parameter  $\tilde{s}$ . It means that the center of the second cluster is located around the fixed position. Later, we will discuss how the spatial correlations between clusters (inter-cluster correlation) can be affected by the Pauli blocking.

We choose  $\tilde{s}_j = \pi(2j - 1)/2\tilde{k}_F$  with  $j = 1$  and  $j = \tilde{k}_F$ , which are the allowed positions  $\tilde{s}_j$  nearest to  $\tilde{x} = 0$  and  $\tilde{x} = \pi$  and corresponds to the smallest and largest inter-cluster ( $\alpha_1$ - $\alpha_2$ ) distances, respectively. The density distribution  $\rho_s^\chi(\tilde{x})$  in the  $2\alpha$ -cluster wave function  $\Psi_s$  are shown in the right panels of Figs. 6 and 7 for  $\tilde{k}_F = 1$  and  $\tilde{k}_F = 2$ . In the strong coupling regime, for instance, the  $(\tilde{k}_F, \tilde{b}) = (1.0, 0.25)$  state, the density shows the clear two peak structure and indicates that two clusters are well isolated without almost no overlap. As the  $\tilde{b}$  increases, the overlap region between clusters gradually increases and the density changes to the oscillation structure, in particular, in the case of  $j = \tilde{k}_F$ . The density oscillation is remarkable, for instance, in the  $(\tilde{k}_F, \tilde{b}) = (1.0, 1.0)$  and  $(\tilde{k}_F, \tilde{b}) = (2.0, 0.75)$  states, which shows the  $2\tilde{k}_F + 1$  periodicity. With further increase of  $\tilde{b}$ , the density oscillation weakens and finally disappears to the uniform density, and the system goes to the Fermi gas limit with the Fermi momentum  $\tilde{k}_F$ .

In the present model, we put the  $\alpha_2$  cluster around the fixed position  $\tilde{s}$ . For more realistic wave functions of two  $\alpha$  clusters, one should extend the model by taking into account the motion of the  $\alpha_2$  cluster relative to the  $\alpha_1$  cluster. Microscopically, it corresponds to superposing  $\psi_{\alpha_2}^s$  with various values of the parameter  $s$  as

$$\psi_{\alpha_2} = \int d\tilde{s} F(\tilde{s}) \psi_{\alpha_2}^s. \quad (22)$$

The spatial correlation between clusters (inter-cluster correlation) is expressed by the weight function  $F(\tilde{s})$ . On the other hand, the correlation between nucleons inside a cluster (inner correlation) is described by the intrinsic structure of a single-cluster wave function of  $\psi_{\alpha_1}$  or  $\psi_{\alpha_2}^s$  determined by the parameters  $\tilde{b}$  and  $\tilde{k}_F$ , and it is given by hand in the present model, where the cluster formation and its intrinsic structure are *a priori* assumed.

Moreover, the wave function should be projected to the total momentum  $K_G = 0$  for the center of mass motion (c.m.m.) of two clusters so that the translational invariance is restored in the finite system.

In the following discussions, we do not treat the  $\alpha_2$ -cluster motion explicitly, but conjecture how the Pauli blocking may restrict the motion of the  $\alpha_2$  cluster and affect to the spatial correlations between clusters (inter-cluster correlations). Since the area of high  $\alpha_1$  density is blocked as mentioned, the  $\alpha_2$  cluster may move in the allowed regions with large  $\mathcal{N}_{\text{PB}}^4(\tilde{s})$ . We assume that the interaction between clusters is weak and the Pauli blocking effect, which acts like an effective repulsion, gives the most important contribution in the relative motion between clusters.

### 1. BEC-like state

Let us consider the strong coupling regime, where the cluster size  $\tilde{b}$  is small enough. The  $\mathcal{N}_{\text{PB}}^4(\tilde{s})$  curve shows a wide open window of the allowed region as in the case of  $(\tilde{k}_F, \tilde{b}) = (1.0, 0.25)$ . Since the Pauli blocking effect is weak, the  $\alpha_2$  can move in the wide allowed region almost freely. It means the strong inner correlation but almost no inter-cluster correlation. In such the uncorrelated cluster state, two clusters may condensate approximately the zero momentum state in the ground state similarly to the BEC phase.

### 2. DW-like state

As the  $\tilde{b}$  increases, the open window for the allowed region closes and  $\alpha_2$  no longer can move freely. Instead, the allowed region becomes discrete, and the  $\alpha_2$ -cluster center may be confined around the allowed  $\tilde{s}$  values,  $\tilde{s}_j = \pi(2j-1)/2\tilde{k}_F$  ( $j = 1, \dots, 2\tilde{k}_F$ ).

For a possible wave function for  $\alpha_2$ , one may consider a superposition of wave functions with  $\tilde{s}_j$  as

$$\psi_{\alpha_2} = \sum_j F(\tilde{s}_j) \psi_{\alpha_2}^{s_j}. \quad (23)$$

As seen in the density distribution  $\rho_s^x(\tilde{x})$  of two cluster states shown in Figs. 6 and 7, the density oscillation shows the  $2\tilde{k}_F + 1$  periodicity for any  $\tilde{s}_j$  values.

The density oscillation can be remarkable provided that the amplitude  $F(\tilde{s}_j)$  for  $j = \tilde{k}_F$  (nearest  $\tilde{s}_j$  to the middle point  $\tilde{x} = \pi$ ) is relatively larger than those for  $\tilde{s}_j$  around  $\tilde{s} = 0$  and  $2\pi$  because of the effective repulsion between clusters due to the Pauli blocking effect. In other words, possible localization of the amplitude  $F(\tilde{s}_j)$  because of the Pauli blocking effect causes the spatial correlation between clusters (inter-cluster correlation). In such the case, the density oscillation shows the clear  $2\tilde{k}_F + 1$  periodicity whose origin is the DW-type correlations. Indeed, the state contains dominantly the coherent  $1p-1h$  components of a  $\pm\tilde{k}_F + 1$  particle and a  $\pm\tilde{k}_F$  hole on the Fermi surface at  $\tilde{k}_F$ . The  $1p-1h$  correlation carries the  $2\tilde{k}_F + 1$  momentum and causes the  $2\tilde{k}_F + 1$  periodicity. This correlation is similar to that of the DW phase. In the weak coupling approximation, the spatial wave function Eq. (11) for an  $\alpha$  cluster is approximated by the dominant  $\tilde{k}_F$  component with a minor mixing of the  $\tilde{k}_F + 1$  component as

$$\phi_0(x) = \frac{1}{\sqrt{2L}} (\cos \tilde{k}_F \tilde{x} + \epsilon \cos(\tilde{k}_F + 1)\tilde{x}). \quad (24)$$

In this approximation, it can be proved that the  $2\alpha$  wave function  $\Psi_s$  for  $j = \tilde{k}_F$  actually contains the dominant DW-type  $1p-1h$  correlation in the particle-hole representation (See appendix B).

In the opposite case that there exists attractive force between clusters, the amplitudes  $F(\tilde{s}_j)$  may gather to smaller  $\tilde{s}_j$ . It corresponds to the exciton(Exc)-type correlations described by the coherent  $1p-1h$  components of a  $\pm\tilde{k}_F + 1$  particle and a  $\mp\tilde{k}_F$  hole on the Fermi surface as described in appendix B. In this case, the  $1p-1h$  carries the momentum  $|\tilde{k}_F + 1 \mp \tilde{k}_F| = 1$ , which suggests that spatial density oscillation is not so remarkable. Indeed, such the feature is seen in the weaker density oscillation in  $\rho_s^x(\tilde{x})$  for  $\tilde{s} = \tilde{s}_j$  ( $j = 1$ ) shown in Fig. 7 (dashed lines in the right panels) for  $\tilde{k}_F = 2$ . We should comment that the system for  $k_F = 1$  is a special case that the small  $\tilde{s}$  region, for instance, the region  $\tilde{s} < \pi/4$  is forbidden and the Exc-type correlations are suppressed.

### 3. BCS-like state

With further increase of  $\tilde{b}$ , the  $\tilde{k}_F$  component becomes more dominant. In the case  $f(\tilde{k}) \ll f(\tilde{k}_F)$  for  $\tilde{k} > \tilde{k}_F$ , the structure of the Pauli allowed area for  $\alpha_2$  approaches the pure periodic one following the periodicity of the  $\alpha_1$  density  $\rho_{\alpha_1}(\tilde{x}) \approx \cos^2(\tilde{k}_F \tilde{x})/\sqrt{\pi}$ . Then, a linear combination of  $\psi_{\alpha_2}^{s_j}$  with an equal weight may be the lowest state to restore

the translational invariance because  $\Psi_s$  for different  $\tilde{s}_j$  may degenerate energetically. It means that the state no longer has the spatial correlation between clusters (inter-cluster correlation) and it corresponds to a BCS-like state. Namely, the BCS-like state has the weak inner correlation and no inter-cluster correlation.

As described in appendix B, in the weak coupling approximation, the total c.m.m. momentum  $K_G = 0$  state projected from the equal weight linear combination of two cluster wave functions  $\Psi_s$  is equivalent to the BCS-like state containing  $2p-2h$  configurations of a  $(\tilde{k}_F + 1, -\tilde{k}_F - 1)$   $\chi_\alpha\chi_\beta$  particle pair and a  $(\tilde{k}_F, -\tilde{k}_F)$   $\chi_\alpha\chi_\beta$  hole pair [see Eq. (C5)]. In the  $2p-2h$  state, all kinds of pairing is coherently mixed so as to keep the spin-isospin symmetry of  $\alpha$  clusters.

#### 4. Fermi-gas state and correlations

In the large  $\tilde{b}$  limit, excited components of  $\tilde{k} > \tilde{k}_F$  vanish and the system goes to the Fermi gas (FG) state with the Fermi surface at  $\tilde{k}_F$ . Needless to say, the FG state has no inner correlation nor inter-cluster correlation. This is nothing but the uncorrelated state. On the other hand, the correlated states are characterized by configurations of excited  $\tilde{k} > \tilde{k}_F$  components. In the weak coupling regime, we can recognize DW-like, Exc-like, BCS-like states, or mixing of them by correlations in  $1p-1h$  and  $2p-2h$  configurations on the Fermi surface.

#### 5. Diagram of structure transitions

As discussed above, in the present schematic model for two clusters on the Fermi gas core in the 1D box, the cluster state is expected to show the BEC-like, the DW/Exc-like, BCS-like, or FG behaviors depending on the cluster size  $\tilde{b}$  and the lowest allowed momentum  $\tilde{k}_F$ . We here assume the criterion to judge a correlation type for a wave function with given  $\tilde{b}$  and  $\tilde{k}_F$  values, and show a diagram of structure transitions on the  $\tilde{b}-\tilde{k}_F$  plane.

For the criterion, we define  $\Delta\tilde{k}$  by the deviation of  $\tilde{k}$  from the lowest allowed momentum  $\tilde{k}_F$ .

$$(\Delta\tilde{k})^2 = \sum_{\tilde{k} \geq \tilde{k}_F} f^2(\tilde{k})(\tilde{k} - \tilde{k}_F)^2. \quad (25)$$

It indicates the deviation from the FG state  $|HF\rangle$ . In the case  $\Delta\tilde{k} \ll 1$ ,  $\tilde{k} \geq \tilde{k}_F + 2$  components are negligible and the coefficient  $\epsilon \equiv f(\tilde{k}_F + 1)$  of the  $\tilde{k}_F + 1$  component approximates  $\epsilon \approx \Delta\tilde{k}$ . In the  $\Delta\tilde{k} = 0$  limit, the system goes to the FG state. For the criterion to classify a wave function with given  $\tilde{b}$  and  $\tilde{k}_F$  to a correlation type, we use the deviation  $\Delta\tilde{k}$  and the Pauli allowedness  $\mathcal{N}_{PB}^4(\tilde{s})$  at the middle point of the box  $\tilde{s} = \tilde{L}/2 = \pi$ .

In Table I, we list the criterion for various correlation types. In the table, we also show the typical examples of the  $\tilde{b}$  values for  $\tilde{k}_F = 1$  and  $\tilde{k}_F = 2$  that satisfy the criterion. The densities and the Pauli allowedness for the corresponding states are already shown in Figs. 6 and 7. The BEC-like state is expected to appear when the Pauli allowed region is widely open. Then, we adopt the condition  $\mathcal{N}_{PB}^4(\tilde{s} = \pi) > 0.8$  for the BEC-like state. The DW-like and/or Exc-like states may appear when the Pauli allowed region is restricted. For this condition, we use  $\mathcal{N}_{PB}^4(\tilde{s} = \pi) < 0.1$ . The DW/Exc-like states may change to the BCS-like state when the  $\alpha_1$ -cluster density  $\rho_{\alpha_1}(x)$  approaches  $\cos^2(\tilde{k}_F x)/\sqrt{\pi}$  and the Pauli allowed area for  $\alpha_2$  becomes almost periodic. For the criterion that  $\rho_{\alpha_1}(\tilde{x}) \approx \cos^2(\tilde{k}_F \tilde{x})/\sqrt{\pi}$ , we adopt the ratio of the  $\alpha_1$  density at  $\tilde{x} = 0$  to that at  $\tilde{x} = \tilde{L}/2 = \pi$ . In the weak coupling regime of  $\Delta\tilde{k} \ll 1$ , the ratio  $\rho_{\alpha_1}^x(\tilde{x} = 0)/\rho_{\alpha_1}^x(\tilde{x} = \pi)$  is approximately given by  $1 - 4\epsilon \approx 1 - 4\Delta\tilde{k}$ , therefore, we use  $\Delta\tilde{k}$  for the measure. We apply  $\Delta\tilde{k} > 0.05$  for the DW/Exc-like states. This approximately corresponds to the ratio  $\rho_{\alpha_1}^x(\tilde{x} = 0)/\rho_{\alpha_1}^x(\tilde{x} = \pi) < 0.8$ . With the decrease of  $\Delta\tilde{k}$ , the  $2\alpha$  wave function may gradually change to the FG state via the BCS-like state. Since the higher momentum components  $\tilde{k} > \tilde{k}_F$  nearly equals to  $(\Delta\tilde{k})^2$  in the weak coupling regime, we use  $\Delta\tilde{k}$  as the measure for structure transitions from the DW/Exc-like to the FG state as listed in the table. For instance, the condition  $\Delta\tilde{k} < 0.001$  for the FG state indicates the contamination of  $\tilde{k} > \tilde{k}_F$  components is less than  $10^{-6}$ .

The diagram of the structure transitions between the FG state, BCS-like state, DW/Exc-like state, and BEC-like state on the  $\tilde{k}_F-\tilde{b}$  plane is shown in Fig. 8.

For a system with higher  $\tilde{k}_F$ , nucleons in a cluster couple more weakly to each other because of Pauli blocking from core nucleons, and therefore the FG region is wider in the diagram. However, one should care about that the assumption of the sharp surface for the core Fermi momentum might be inadequate, in particular, in case of high  $\tilde{k}_F$ . The core Fermi surface may diffuse in correlated states. If the surface diffuses, the lower orbitals below  $\tilde{k}_F$  are partially allowed for nucleons in clusters. Then, the weakening of the cluster localization by the Pauli blocking from core nucleons can be quenched. The present model should be extended by incorporating the surface diffuseness of the core Fermi surface.

TABLE I: For the criterion to classify the 1D-cluster wave function with given  $\tilde{b}$  and  $\tilde{k}_F$  into various types of correlation. The deviation  $\Delta\tilde{k}$  and the Pauli allowedness  $\mathcal{N}_{PB}^4(\tilde{s} = \tilde{L}/2 = \pi)$  are used for the criterion. The typical examples of the  $\tilde{b}$  values for  $\tilde{k}_F = 1$  and  $\tilde{k}_F = 2$  that satisfy the criterion are also shown in the table.

correlation	criterion	example
		$\tilde{k}_F = 1$ $\tilde{k}_F = 2$
FG	$\Delta\tilde{k} < 0.001$	$\tilde{b} = 2.0$
FG-BCS crossover	$0.001 \leq \Delta\tilde{k} < 0.005$	$\tilde{b} = 2.0$ $\tilde{b} = 1.5$
BCS-like	$0.005 \leq \Delta\tilde{k} < 0.01$	
BCS-DW/Exc crossover	$0.01 \leq \Delta\tilde{k} < 0.05$	$\tilde{b} = 1.5$ $\tilde{b} = 1.25$
DW/Exc-like	$0.05 \leq \Delta\tilde{k}$ and $\mathcal{N}_{PB}^4(\tilde{L}/2) < 0.1$	$\tilde{b} = 1.0$ $\tilde{b} = 0.75$
DW/Exc-BEC crossover	$0.1 \leq \mathcal{N}_{PB}^4(\tilde{L}/2) < 0.8$	$\tilde{b} = 0.5$ $\tilde{b} = 0.5$
BEC-like	$0.8 < \mathcal{N}_{PB}^4(\tilde{L}/2)$	$\tilde{b} = 0.25$ $\tilde{b} = 0.25$

We also should comment that, in a real system, two parameters  $\tilde{b}$  and  $\tilde{k}_F$  are uncontrollable in general. As explained before,  $\tilde{b}$  indicates the cluster size relative to the box size (the cluster density), while  $\tilde{k}_F$  relates to the core density. The size of clusters on the Fermi gas core should be determined dynamically as a consequence of nuclear interactions between constituent nucleons in clusters. It should be also affected by the neighboring cluster, i.e., cluster density as well as  $\tilde{k}_F$ . Moreover, the ratio of cluster nucleons to the core nucleons should be determined dynamically. The extension of the present model by taking into account dynamical change of cluster structure with the use of effective nuclear interactions is an important issue to be solved in future study.

## F. Correspondence to finite nuclei

As shown in the AMD+VAP calculation, three  $\alpha$  clusters are formed in the ground state of  $^{12}\text{C}$  even though the existence of any clusters is not *a priori* assumed in the framework. Once three  $\alpha$  clusters are formed, it can be associated with the schematic 1D-cluster model. Angular correlation between two  $\alpha$  clusters around the  $\alpha$  core corresponds to the spatial correlation between two  $\alpha$  clusters in the 1D-cluster model with  $\tilde{k}_F = 1$ . The cluster size  $b$  is 1.62 fm for  $\nu = 0.19 \text{ fm}^{-2}$  used in the AMD calculations. If we adopt the r.m.s. matter radius  $r_\alpha = 1.72$  fm of the core  $\alpha$  as the radial size  $r_0$ , the dimensionless  $\tilde{b} = b/r_0$  is estimated to be  $\tilde{b} = 0.94$ . Or if we use the r.m.s. radius of cluster positions of 3  $\alpha$ s evaluated from  $r_0^2 + r_\alpha^2 = R_0^2$ , we get  $\tilde{b} = 0.87$ . In both cases,  $\tilde{b} \sim 1$ . As already described, the state with  $(\tilde{k}_F, \tilde{b}) = (1.0, 1.0)$  in the 1D-cluster model shows the remarkable density oscillation with the wave number three in the DW-like regime. It is consistent with the intrinsic structure with the  $^{12}\text{C}(0_1^+)$  obtained with the AMD+VAP calculation. Indeed, the  $^{12}\text{C}(0_1^+)$  has the  $(Y_3^{-3} - Y_3^{+3})/\sqrt{2}$  component and the surface density shown in Fig. 2 is similar to the oscillating density in the 1D-cluster state for  $(\tilde{k}_F, \tilde{b}) = (1.0, 1.0)$  in Fig. 6.

As discussed in Ref. [37], the  $\alpha$  correlation in the pentagon ground state of  $^{28}\text{Si}$  can be interpreted as the density wave on the *sd*-shell oblate state. The  $^{28}\text{Si}$  ground state is associated with the 1D-cluster model with  $\tilde{k}_F = 2$  considering a core consisting of the spherical  $^{16}\text{O}$  and four nucleons in oblate orbits. Then, the pentagon shape can be understood again by the DW-like state in the 1D-cluster model wave function with the  $2\tilde{k}_F + 1 = 5$  periodicity.

In case of the  $\alpha$  correlation in the  $^{16}\text{O}$  ground state, the tetrahedron shape can not be connected directly to the 1D problem. However, when we focus only on the  $(Y_3^{-3} - Y_3^{+3})/\sqrt{2}$  component of the intrinsic density in the  $^{16}\text{O}$  ground state, the density oscillation is characterized by the wave number three periodicity similar to that of the triangle shape in  $^{12}\text{C}(0_1^+)$  and the deformation feature is associated with the DW-type correlation in the 1D cluster model as in  $^{12}\text{C}$ .

## V. SUMMARY AND OUTLOOK

We investigated  $\alpha$ -cluster correlations in the ground states of  $^{12}\text{C}$  and  $^{16}\text{O}$  while focusing on the surface density oscillation in the intrinsic states. The intrinsic states of  $^{12}\text{C}$  and  $^{16}\text{O}$  obtained by the AMD+VAP method show triangle and tetrahedral shapes, respectively, because of the  $\alpha$  correlations. The formation of  $\alpha$  clusters in these states was confirmed in the AMD framework, in which existence of any clusters are not *a priori* assumed. The intrinsic deformations are regarded as spontaneous symmetry breaking of rotational invariance. It was shown that

the oscillating surface density in the triangle and tetrahedral shapes is associated with that in DW states caused by the instability of Fermi surface with respect to a kind of  $1p-1h$  correlations.

To discuss the symmetry breaking between uniform density states and the oscillating density states, a schematic model of a few clusters on a Fermi gas core in a one-dimensional finite box was introduced. In the model analysis, we conjecture structure transitions from a Fermi gas state to a DW-like state via a BCS-like state, and to a BEC-like state depending on the cluster size relative to the box size.

In both analyses of the BB-cluster model and the schematic 1D-cluster model, Pauli blocking effects are found to play an important role in the DW-like state. The breaking of the translational invariance in the DW-like state originates in the Pauli blocking effect between clusters, which acts as an effective inter-cluster repulsion and restricts cluster motion.

In the present analysis with the schematic 1D-cluster model, we do not perform energy variation nor calculate energy eigenstates. Moreover, the mechanism of cluster formation and the dynamical change of the cluster structure or the cluster size are beyond our scope in the present paper. The extension of the present model by taking into account dynamical change of cluster structure with the use of effective nuclear interactions is an important issue to be solved in future study. Also the cluster and core formations as well as diffuseness of the core Fermi surface should be studied in more realistic models. Furthermore, the assumption that the interaction between clusters is weak and the Pauli blocking effect gives the major contribution to the inter-cluster motion may be too simple. To clarify which state of BCS-like, DW-like, or EXc-like ones realizes it is essential to explicitly solve the problem of inter-cluster motion by taking into account nuclear forces or inter-cluster interactions.

It would be interesting to associate the present picture for clusters in the 1D finite box with phase transitions in infinite matter. In the extension of the present model to infinite matter problem, one should take care of the differences between finite systems and infinite systems as follows. Firstly, momentum  $k$  values in a finite box is discrete because of boundary condition, while they are continuum values in infinite matter. In the description with discrete momentum, long range correlations beyond the box size  $L$  is not taken into account. What we call the BCS-type correlation in the present 1D-cluster model is the correlation in the range of the box size at most. In second, the total momentum of c.m.m. should be projected to zero in finite system, while it is not necessarily zero in infinite systems. In spite of those differences, the 1D-cluster model may give a hint to understand an origin of DW in infinite matter.

### Acknowledgments

The authors thank to nuclear theory group members of department of physics of Kyoto University for valuable discussions. Discussions during the YIPQS long-term workshop "DCEN2011" held at YITP are helpful to advance this work. The computational calculations of this work were performed by using the supercomputers at YITP. This work was supported by Grant-in-Aid for Scientific Research from Japan Society for the Promotion of Science (JSPS) Grant Number [No.23340067, 24740184]. It was also supported by the Grant-in-Aid for the Global COE Program "The Next Generation of Physics, Spun from Universality and Emergence" from the Ministry of Education, Culture, Sports, Science and Technology (MEXT) of Japan.

### Appendix A: Triangle and tetrahedral deformations in the $3\alpha$ - and $4\alpha$ -cluster structures

We here describe triangle and tetrahedral deformations and particle-hole representations of  $3\alpha$ - and  $4\alpha$ -cluster wave functions. As explained in Ref. [37], the Brink-Bloch (BB)  $3\alpha$ -cluster wave functions [53] with a regular triangle configuration in the small inter-cluster distance case can be rewritten as,

$$\Phi_{3\alpha}^{BB}(\epsilon) \approx \prod_{\tau\sigma} \{ \phi_{00} \mathcal{X}_{\tau\sigma}(\phi_{1-1} + \epsilon\phi_{2+2}) \mathcal{X}_{\tau\sigma}(\phi_{1+1} - \epsilon\phi_{2-2}) \mathcal{X}_{\tau\sigma} \}. \quad (\text{A1})$$

Here  $\phi_{lm}$  is the single-particle orbit in the harmonic oscillator potential,  $\mathcal{X}_{\tau\sigma}$  is the spin-isospin wave function with  $\tau = \{p, n\}$  and  $\sigma = \{\uparrow, \downarrow\}$ .  $\epsilon$  is the order parameter for the axial symmetry breaking and it corresponds to  $u/v$  in the BCS theory. Here  $\epsilon$  is considered to be small to omit  $\epsilon^2$  and higher terms and taken to be a real value. In principle,  $\epsilon$  can be a complex value but the phase is arbitrary and can be changed by the rotation around the  $z$  axis (transformation of the polar coordinate  $\varphi$ ). The density of the  $\Phi_{3\alpha}^{BB}(\epsilon)$  state is

$$\rho(\mathbf{r}) = \frac{4}{\pi^{3/2} b^3} e^{-\frac{r^2}{b^2}} \left\{ 1 + 2 \frac{r^2}{b^2} \sin^2(\theta) + \epsilon 2\sqrt{2} \frac{r^3}{b^3} \sin^3(\theta) (e^{-3i\varphi} - e^{3i\varphi}) + \mathcal{O}(\epsilon^2) \right\}, \quad (\text{A2})$$

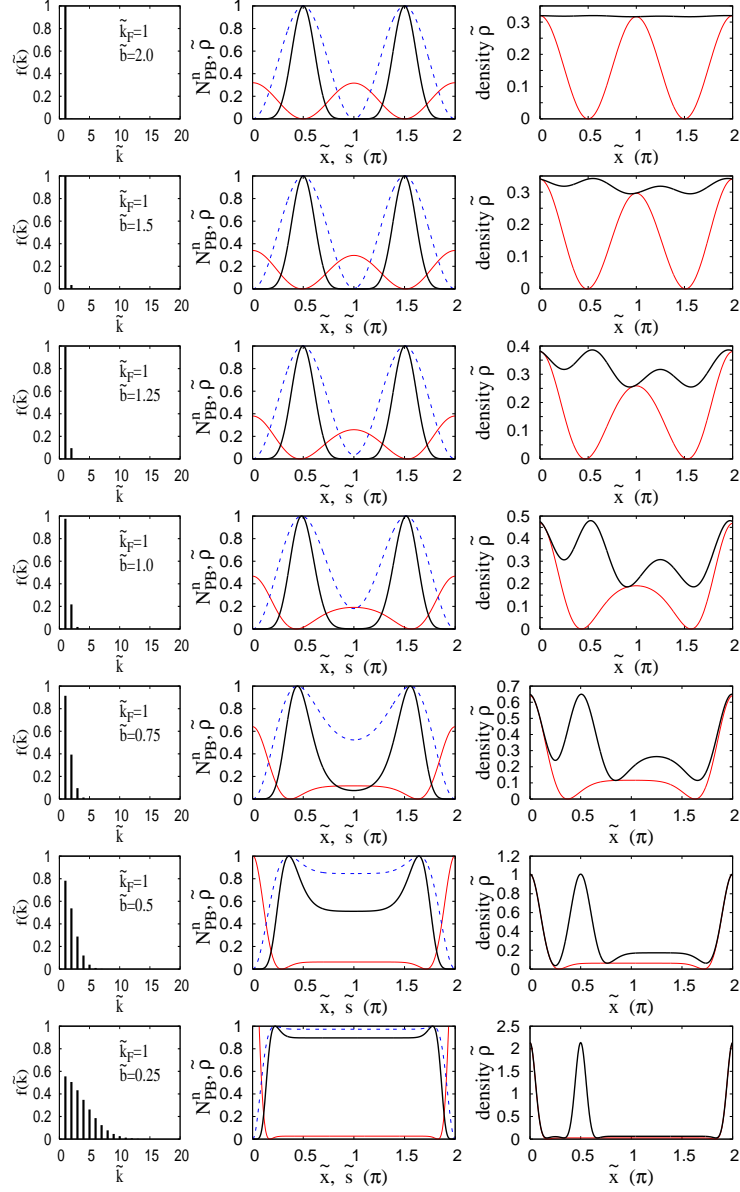


FIG. 6: (Color on-line) The results of one and two clusters on the Fermi gas core in a one-dimension box. Left: The coefficients  $f(\tilde{k})$  of the Fourier transformation. Middle: The density  $\rho_{\alpha_1}^x(\tilde{x})$  of the first  $\alpha$  located around  $\tilde{x} = 0$  (red thin lines), the PB effect  $\mathcal{N}_{PB}^{\alpha_1}(\tilde{s})$  for the second  $\alpha$  (black solid lines).  $\mathcal{N}_{PB}^{\alpha_1}(\tilde{s})$  is also shown (blue dashed lines). Right: The density  $\rho_s^x(\tilde{x})$  (black solid lines). The  $\tilde{s}$  for the center position of  $\alpha_2$  is chosen to be  $\tilde{s}_j$  with  $j = \tilde{k}_F$ , which is the closest  $\tilde{s}_j$  to  $\tilde{x} = \tilde{L}/2 = \pi$  among the allowed  $\tilde{s}$  values. The density  $\rho_{\alpha_1}^x(\tilde{x})$  is also shown for comparison (red thin lines). The results for the cluster size  $\tilde{b} = 2.0, 1.5, 1.25, 1.0, 0.75, 0.5, 0.25$  are shown.

and its multipole decomposition at a certain radius  $r = R_0$  is

$$\rho(R_0, \theta, \varphi) = \frac{8}{\pi^{1/2} b^3} e^{-\frac{R_0^2}{b^2}} \left\{ \left( 1 + \frac{4 R_0^2}{3 b^2} \right) Y_0^0(\theta, \varphi) - \frac{4 R_0^2}{3\sqrt{5} b^2} Y_2^0(\theta, \varphi) + \epsilon \frac{8 R_0^3}{\sqrt{35} b^3} \left( \frac{Y_3^{-3}(\theta, \varphi)}{\sqrt{2}} - \frac{Y_3^{+3}(\theta, \varphi)}{\sqrt{2}} \right) + \mathcal{O}(\epsilon^2) \right\}. \quad (\text{A3})$$

In a similar way, the BB  $4\alpha$ -cluster wave functions with a regular tetrahedral configuration can be rewritten as

$$\Phi_{4\alpha}^{BB}(\epsilon) \approx \prod_{\tau\sigma} \{ \phi_{00} \mathcal{X}_{\tau\sigma} \phi_{10} \mathcal{X}_{\tau\sigma} (\phi_{1-1} + \epsilon \phi_{2+1}) \mathcal{X}_{\tau\sigma} (\phi_{1+1} + \epsilon \phi_{2-1}) \mathcal{X}_{\tau\sigma} \}. \quad (\text{A4})$$

Here it is assumed that the inter-cluster distance in the tetrahedral configuration is small, i.e.,  $\epsilon$  is small. The density

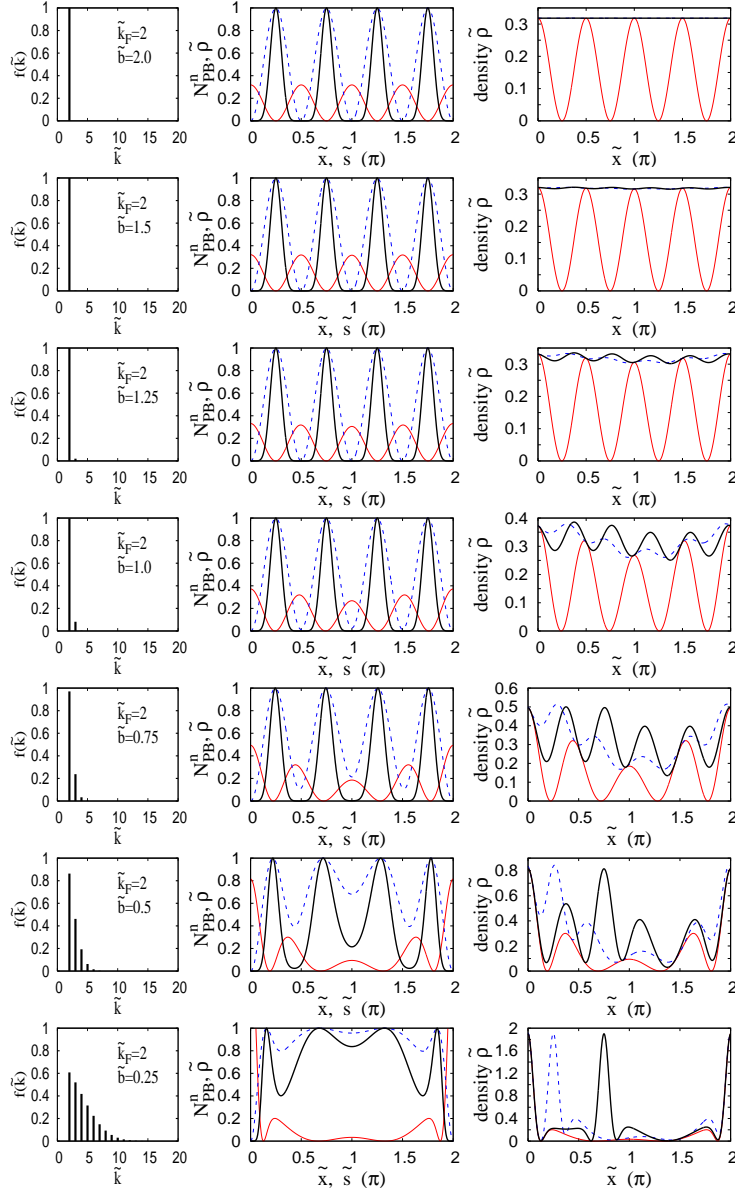


FIG. 7: Same as Fig. 6 but for  $\tilde{k}_F = 2$ . The blue dashed lines indicate the the density  $\rho_s^{\tilde{x}}(\tilde{x})$  for the smallest allowed  $\tilde{s}$  value,  $\tilde{s}_j$  with  $j = 1$ . The results for the cluster size  $\tilde{b} = 2.0, 1.5, 1.25, 1.0, 0.75, 0.5, 0.25$  are shown.

is

$$\rho(\mathbf{r}) = \frac{4}{\pi^{3/2} b^3} e^{-\frac{r^2}{b^2}} \left\{ 1 + 2 \frac{r^2}{b^2} \sin^2(\theta) + \epsilon \sqrt{2} \frac{r^3}{b^3} \sin^2(\theta) (e^{2i\varphi} + e^{-2i\varphi}) + \mathcal{O}(\epsilon^2) \right\}, \quad (\text{A5})$$

and its multipole decomposition at a radius  $r = R_0$  is

$$\rho(R_0, \theta, \varphi) = \frac{8}{\pi^{1/2} b^3} e^{-\frac{R_0^2}{b^2}} \left\{ \left( 1 + 2 \frac{R_0^2}{b^2} \right) Y_0^0(\theta, \varphi) + \epsilon \sqrt{\frac{32}{105}} \frac{R_0^3}{b^3} \left( \frac{Y_3^{-2}(\theta, \varphi)}{\sqrt{2}} + \frac{Y_3^{+2}(\theta, \varphi)}{\sqrt{2}} \right) \right\}. \quad (\text{A6})$$

$Y_3^{-2}(\theta, \varphi)/\sqrt{2} + Y_3^{+2}(\theta, \varphi)/\sqrt{2}$  in the  $\epsilon$  term can be also transformed to

$$\frac{Y_3^{-2}(R_\Omega \theta', R_\Omega \varphi')}{\sqrt{2}} + \frac{Y_3^{+2}(\theta', \varphi')}{\sqrt{2}} = \frac{\sqrt{5}}{3} Y_3^0(\theta, \varphi) + \frac{\sqrt{2}}{3} Y_3^{-3}(\theta, \varphi) - \frac{\sqrt{2}}{3} Y_3^{+3}(\theta, \varphi), \quad (\text{A7})$$

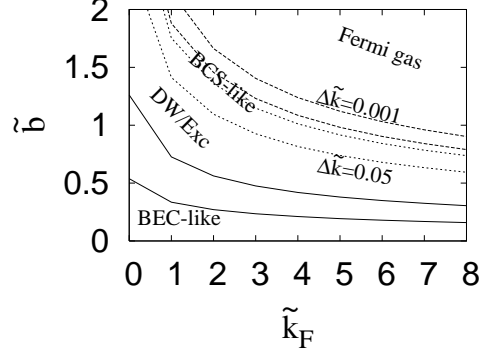


FIG. 8: Diagram of structure transitions between the Fermi gas state, BCS-like state, DW/Exc-like state, and BEC-like state in the schematic 1D-cluster model. The criterion for the boundary are listed in I. The conditions of  $\mathcal{N}_{PB}^4(\tilde{L}/2) = 0.1$  and  $0.8$  are shown by the solid lines, while the conditions of  $\Delta\tilde{k} = 0.001, 0.005, 0.01, 0.05$  are shown by the dashed lines.

by a  $\Omega$  rotation  $R_\Omega$ .

By using the creation and annihilation operators,  $a_{lm,\chi}^\dagger$  and  $a_{lm,\chi}$  for the  $\phi_{lm}\mathcal{X}_{\tau\sigma}$  state with  $\chi = \tau\sigma$ , the  $\Phi_{3\alpha}^{BB}(\epsilon)$  and  $\Phi_{4\alpha}^{BB}(\epsilon)$  states are expressed as

$$|\Phi_{3\alpha}^{BB}(\epsilon)\rangle = \prod_{\chi} a_{00,\chi}^\dagger (a_{1-1,\chi} + \epsilon a_{2+2,\chi}^\dagger) (a_{1+1,\chi} - \epsilon a_{2-2,\chi}^\dagger) |-\rangle, \quad (\text{A8})$$

$$|\Phi_{4\alpha}^{BB}(\epsilon)\rangle = \prod_{\chi} a_{00,\chi}^\dagger a_{10,\chi}^\dagger (a_{1-1,\chi} + \epsilon a_{2+1,\chi}^\dagger) (a_{1+1,\chi} + \epsilon a_{2-1,\chi}^\dagger) |-\rangle. \quad (\text{A9})$$

In the particle and hole representation, they are rewritten as

$$|\Phi_{3\alpha}^{BB}(\epsilon)\rangle = \prod_{\chi} (1 + \epsilon a_{2+2,\chi}^\dagger b_{1+1,\chi}^\dagger) (1 - \epsilon a_{2-2,\chi}^\dagger b_{1-1,\chi}^\dagger) |0\rangle_F, \quad (\text{A10})$$

$$|0\rangle_F \equiv \prod_{\chi} (a_{00,\chi}^\dagger a_{1-1,\chi} a_{1+1,\chi}) |-\rangle, \quad (\text{A11})$$

and

$$|\Phi_{4\alpha}^{BB}(\epsilon)\rangle = \prod_{\chi} (1 + \epsilon a_{2+1,\chi}^\dagger b_{1+1,\chi}^\dagger) (1 + \epsilon a_{2-1,\chi}^\dagger b_{1-1,\chi}^\dagger) |0\rangle_F, \quad (\text{A12})$$

$$|0\rangle_F \equiv \prod_{\chi} (a_{00,\chi}^\dagger a_{10,\chi}^\dagger a_{1-1,\chi} a_{1+1,\chi}) |-\rangle. \quad (\text{A13})$$

Here the hole operator  $b_{lm,\chi}^\dagger$  is defined to be  $b_{lm,\chi}^\dagger = a_{l-m,\chi}$ . Equations (A10) and (A12) indicate that the  $3\alpha$ - and  $4\alpha$ -cluster wave functions contains the DW-type  $1p$ - $1h$  correlations carrying finite angular momenta.

## Appendix B: Weak coupling regime of one-dimensional cluster model

We consider the weak-coupling case of the 1D-cluster model described in IV. Hereafter, we take  $r_0 = 1$  and consider the case that all the parameters equal to the dimensionless parameters, for instance,  $b = \tilde{b}$ ,  $k = \tilde{k}$ , and  $s = \tilde{s}$ . We define the creation and annihilation operators  $a_{k\chi}^\dagger$  and  $a_{-k\chi}^\dagger$  for the single-particle states  $\phi_k\mathcal{X}_\chi$  and  $\phi_{-k}\mathcal{X}_\chi$ , where  $\phi_k$  and  $\phi_{-k}$  are momentum  $k$  and  $-k$  plane waves written as  $\phi_k(x) = e^{+ikx}/\sqrt{2L}$  and  $\phi_{-k}(x) = e^{-ikx}/\sqrt{2L}$  in the coordinate representation. The core state  $|C\rangle$  where all  $k < k_F$  states are occupied by core nucleons is written as

$$|C\rangle = \prod_{\chi} \prod_{|k| < k_F} a_{k_F\chi}^\dagger a_{-k_F\chi}^\dagger |-\rangle, \quad (\text{B1})$$

where  $|-\rangle$  is the vacuum.

In the case of weak coupling, the coefficient  $f(k)$  of the momentum  $k$  and  $-k$  plane waves in Eq. (9) is dominant for  $k = k_F$  and it rapidly decreases as  $k$  increases. In the limit,  $|f(k_F)| \gg |f(k_F + 1)| \gg |f(k_F + 2)| \cdots$ , the leading term of the  $2\alpha$ -cluster state in the 1D-cluster model is the Fermi gas state with the surface momentum  $k_F$ , which is the uncorrelated state. For the correlated system, the deviation from the Fermi gas state is important. We take into account the next leading term,  $k = k_F + 1$  components, and ignore the higher momentum components for  $k \geq k_F + 2$ . We set  $f(k_F) = 1$  and  $f(k_F + 1) = \epsilon$  with  $\epsilon \ll 1$  and take the leading term of  $\epsilon$ . Then the state consisting of two  $\alpha$  clusters around  $x = 0$  and  $x = s$  written by Eqs. (9) and (14) on the Fermi gas core is expressed as

$$\begin{aligned} |\psi_{\alpha_1} \psi_{\alpha_2}^s C\rangle &\propto \prod_{\chi} \left\{ (c_0^* - c_0) a_{k_F \chi}^\dagger a_{-k_F \chi}^\dagger \right. \\ &\quad + \epsilon (c_0 - c_1) a_{k_F \chi}^\dagger a_{k_F \chi}^\dagger + \epsilon (c_0^* - c_1^*) a_{-k_F \chi}^\dagger a_{-k_F \chi}^\dagger \\ &\quad + \epsilon (c_0^* - c_1) a_{k_F \chi}^\dagger a_{-k_F \chi}^\dagger + \epsilon (c_0 - c_1^*) a_{-k_F \chi}^\dagger a_{k_F \chi}^\dagger \\ &\quad \left. + \epsilon^2 (c_1^* - c_1) a_{k_F \chi}^\dagger a_{-k_F \chi}^\dagger + \cdots \right\} |C\rangle, \end{aligned} \quad (\text{B2})$$

where  $k_F' = k_F + 1$ ,  $c_0(s) = e^{-ik_F s}$ , and  $c_1(s) = e^{-ik_F' s}$ . The first term is the Fermi gas state with the Fermi surface at  $k_F$ . Its coefficient  $c_0^* - c_0 = 2i \sin(k_F s)$  vanishes for  $s = \pi m / k_F$  ( $m$  is an integer) because of Pauli principle. In other words, the area around  $s = \pi 2m / 2k_F$  ( $m = 0, \dots, 2k_F$ ) is forbidden for the  $\alpha_2$  cluster center position, while the area around  $s_j = \pi(2j - 1) / 2k_F$  ( $j = 1, \dots, 2k_F$ ) is allowed.

In the particle-hole representation with respect to the Fermi surface at  $k_F$ , the second and third terms correspond to the  $1p - 1h$  states with the DW-type correlation with the wave number  $k_F' + k_F = 2k_F + 1$ , and the fourth and fifth terms are those with the Exc-type correlation with the wave number  $k_F' - k_F = 1$ , and the last term is the  $2p - 2h$  state. We rewrite the coefficients in  $|\psi_{\alpha_1} \psi_{\alpha_2}^s C\rangle$  as

$$\begin{aligned} |\psi_{\alpha_1} \psi_{\alpha_2}^s C\rangle &= n_0^2 \prod_{\chi} C_0(s) \left\{ a_{k_F \chi}^\dagger a_{-k_F \chi}^\dagger \right. \\ &\quad + \epsilon C_{DW}(s) a_{k_F \chi}^\dagger a_{k_F \chi}^\dagger + \epsilon C_{DW}^*(s) a_{-k_F \chi}^\dagger a_{-k_F \chi}^\dagger \\ &\quad + \epsilon C_{Exc}(s) a_{k_F \chi}^\dagger a_{-k_F \chi}^\dagger + \epsilon C_{Exc}^*(s) a_{-k_F \chi}^\dagger a_{k_F \chi}^\dagger \\ &\quad \left. + \epsilon^2 C_2(s) a_{k_F \chi}^\dagger a_{-k_F \chi}^\dagger + \cdots \right\} |C\rangle, \end{aligned} \quad (\text{B3})$$

$$C_0(s) \equiv c_0^* - c_0 = -2i \sin(k_F s), \quad (\text{B4})$$

$$C_{DW}(s) \equiv \frac{c_0 - c_1}{c_0^* - c_0} = \frac{e^{-is} - 1}{2}, \quad (\text{B5})$$

$$C_{Exc}(s) \equiv \frac{c_0^* - c_1}{c_0^* - c_0} = \frac{e^{-is} + 1}{2}, \quad (\text{B6})$$

$$C_2(s) \equiv \frac{c_1^* - c_1}{c_0^* - c_0} = \cos(is). \quad (\text{B7})$$

By using the hole operator  $b_{k\chi}^\dagger = a_{-k\chi}$  we obtain

$$\begin{aligned} |\psi_{\alpha_1} \psi_{\alpha_2}^s C\rangle &= n_0^2 \prod_{\chi} C_0(s) \left\{ 1 \right. \\ &\quad - \epsilon C_{DW}(s) a_{k_F \chi}^\dagger b_{k_F \chi}^\dagger + \epsilon C_{DW}^*(s) a_{-k_F \chi}^\dagger b_{-k_F \chi}^\dagger \\ &\quad + \epsilon C_{Exc}(s) a_{k_F \chi}^\dagger b_{-k_F \chi}^\dagger - \epsilon C_{Exc}^*(s) a_{-k_F \chi}^\dagger b_{k_F \chi}^\dagger \\ &\quad \left. + \epsilon^2 C_2(s) a_{k_F \chi}^\dagger a_{-k_F \chi}^\dagger b_{-k_F \chi}^\dagger b_{k_F \chi}^\dagger + \cdots \right\} |HF\rangle, \end{aligned} \quad (\text{B8})$$

where the Hartree-Fock vacuum  $|HF\rangle \equiv \prod_{\chi} a_{k_F \chi}^\dagger a_{-k_F \chi}^\dagger |C\rangle$ . When  $s$  is the allowed  $s_j$  close to  $L/2 = \pi$ , i.e., the  $\alpha_2$  center is located around the middle of the box,  $e^{-is}$  approaches  $-1$ , and therefore, the DW correlation becomes dominant and the Exc correlation is minor, while they are opposite for  $s_j$  close to 0. In both cases, the correlation disappears in the  $\epsilon \rightarrow 0$  limit, and the system goes to the Fermi gas limit.

### Appendix C: Transition between DW/Exc-like and BCS-like states

We extend the model in the weak coupling limit described in the previous section by superposing all allowed  $s_j$  states for the  $\alpha_2$  wave function,

$$\psi_{\alpha_2} = \sum_j F(s_j) \psi_{\alpha_2}^{s_j}, \quad (\text{C1})$$

$$|\Psi\rangle = \sum_j F(s_j) |\psi_{\alpha_1} \psi_{\alpha_2}^{s_j} C\rangle. \quad (\text{C2})$$

In principle, one should determine the coefficients  $F(s_j)$  following the energy variation to properly take into account dynamics of relative motion between clusters,  $\alpha_1$  and  $\alpha_2$ . However, we here do not perform energy optimization but adopt a simple ansatz for  $F(s_j)$  as follows.

As described before, if the  $s_j \sim L/2$  ( $s_j \sim 0$ ) components are main, the DW (Exc) correlation is dominant. In more general, in case that the effective interaction between  $\alpha$  clusters is repulsive, the amplitudes may be relatively smaller in the region around  $s_j \sim 0$  (and also around  $s_j \sim L$  due to the periodic boundary) than that around  $s_j = L/2 = \pi$  resulting in the DW dominance. On the other hand, if the interaction between  $\alpha$  clusters is attractive, the amplitudes concentrate on the region around  $s_j \sim 0$ , which may cause the Exc dominance. In both cases, spatial correlation between  $\alpha_1$  and  $\alpha_2$  remains and the system shows density oscillation and the symmetry breaking of translational invariance.

Next we construct the state where there is no spatial correlation between  $\alpha_1$  and  $\alpha_2$  (no inter-cluster correlation) and the translational invariance is completely restored by the superposition and the  $K_G = 0$  (total momentum of c.m.m.) projection of the  $|\psi_{\alpha_1} \psi_{\alpha_2}^{s_j} C\rangle$ . The state with no spacial correlation between  $\alpha_1$  and  $\alpha_2$  can be constructed by the projection to the relative momentum  $k_{\alpha_1} - k_{\alpha_2} = 0$  state. Here  $k_{\alpha_{1,2}}$  stands for the momentum of c.m.m. of  $\alpha_{1,2}$ . In the weak coupling regime, this is performed by superposing all allowed  $s_j$  states with an equal weight as

$$\psi_{\alpha_2} = \sum_j \frac{1}{(-2i(-1)^j)^n} \psi_{\alpha_2}^{s_j}. \quad (\text{C3})$$

Taking averages of  $C_{DW}(j)$ ,  $C_{Exc}(j)$  and  $C_2(j)$  with respect to  $j$ , we obtain

$$\begin{aligned} |\psi_{\alpha_1} \psi_{\alpha_2} C\rangle \propto \prod_{\chi} \left\{ 1 - \frac{\epsilon}{2} (a_{k'_F \chi}^\dagger b_{k_F \chi}^\dagger - a_{-k'_F \chi}^\dagger b_{-k_F \chi}^\dagger) \right. \\ \left. - \frac{\epsilon}{2} (a_{k'_F \chi}^\dagger b_{-k_F \chi}^\dagger - a_{-k'_F \chi}^\dagger b_{k_F \chi}^\dagger) + \dots \right\} |HF\rangle, \end{aligned} \quad (\text{C4})$$

This corresponds to the intrinsic state for no correlation between clusters. In the ground state of the finite system, the total momentum  $K_G = k_{\alpha_1} + k_{\alpha_2}$  should be zero. With the projection onto  $K_G = 0$ , we finally obtain the symmetry restored state,

$$P^{K_G=0} |\psi_{\alpha_1} \psi_{\alpha_2} C\rangle \propto \left\{ 1 + \frac{\epsilon^2}{4} \sum_{\chi_\alpha \chi_\beta} (a_{k'_F \chi_\alpha}^\dagger a_{-k'_F \chi_\beta}^\dagger - a_{k'_F \chi_\beta}^\dagger a_{-k'_F \chi_\alpha}^\dagger) (b_{k_F \chi_\alpha}^\dagger b_{-k_F \chi_\beta}^\dagger - b_{k_F \chi_\beta}^\dagger b_{-k_F \chi_\alpha}^\dagger) + \dots \right\} |HF\rangle. \quad (\text{C5})$$

It is found that the state contains  $2p$ - $2h$  configurations and it is consistent with a BCS-like state, where two particles form a  $(k'_F, -k'_F)$   $\chi_\alpha \chi_\beta$  pair and two holes do a  $(k_F, -k_F)$   $\chi_\alpha \chi_\beta$  pair. In the  $2p$ - $2h$  state, all kinds of  $\chi$  pairing is coherently mixed so as to keep the spin-isospin symmetry originating in the symmetry of  $\alpha$  clusters.

Note that, in the inter-cluster correlated case of the DW dominance state, the  $K_G = 0$  projected state contains  $a_{k'_F \chi_\alpha}^\dagger a_{-k'_F \chi_\beta}^\dagger b_{k_F \chi_\alpha}^\dagger b_{-k_F \chi_\beta}^\dagger + a_{k'_F \chi_\beta}^\dagger a_{-k'_F \chi_\alpha}^\dagger b_{k_F \chi_\beta}^\dagger b_{-k_F \chi_\alpha}^\dagger$  in the  $\epsilon^2$  term, which means that  $1p$ - $1h$  of  $\chi_\alpha$  always carries the finite momentum  $\pm(k'_F + k_F)$  as a result of spatial correlation between clusters.

### References

---

[1] J. A. Wheeler, Phys. Rev. **52**, 1083 (1937); *ibid.* **52**, 1107 (1937).

- [2] D. M. Dennison, Phys. Rev. **96**, 378 (1954).
- [3] D. M. Brink, H. Friedrich, A. Weiguny and C. W. Wong, Phys. Lett. **B33**, 143 (1970).
- [4] K. Ikeda *et al.*, Prog. Theor. Phys. Suppl. **52**, 1 (1972).
- [5] H. Horiuchi, Prog. Theor. Phys. **51**, 1266 (1974); **53**, 447 (1975).
- [6] Yu. F. Smirnov, I. T. Obukhovskiy, Yu. M. Tchuvil'skiy and V. G. Neudatchin, Nucl. Phys. A **235**, 289 (1974).
- [7] E. Uegaki, S. Okabe, Y. Abe and H. Tanaka, Prog. Theor. Phys. **57**, 1262 (1977). E. Uegaki, Y. Abe, S. Okabe and H. Tanaka, Prog. Theor. Phys. **59**, 1031 (1978); **62**, 1621 (1979).
- [8] Y. Fukushima and M. Kamimura, *Proc. Int. Conf. on Nuclear Structure, Tokyo, 1977, edited by T. Marumori*[J. Phys. Soc. Jpn. **44**, 225 (1978); M. Kamimura, Nucl. Phys. **A351**, 456 (1981).
- [9] Y. Suzuki, Prog. Theor. Phys. **55**, 1751 (1976).
- [10] Y. Fujiwara *et al.*, Prog. Theor. Phys. Suppl. **68**, 29 (1980).
- [11] W. Bauhoff, H. Schultheis, R. Schultheis Phys. Rev. **C 29**, 1046 (1984).
- [12] Y. Abe, J. Hiura and H. Tanaka, Prog. Theor. Phys. **46**, 352 (1971); *ibid.* **49**, 800 (1972).
- [13] N. Takigawa and A. Arima, Nucl. Phys. A **168**, 593 (1971).
- [14] A. Tohsaki, H. Horiuchi, P. Schuck, and G. Röpke, Phys. Rev. Lett. **87**, 192501 (2001).
- [15] G. Röpke, A. Schnell, P. Schuck, and P. Nozieres, Phys. Rev. Lett. **80**, 3177 (1998).
- [16] A. W. Overhauser, Phys. Rev. Lett. **4**, 415 (1960).
- [17] D. M. Brink and J. J. Castro, Nucl. Phys. **A216**, 109 (1973).
- [18] M. de Llano, Nucl. Phys. A **317**, 183 (1979).
- [19] H. Ui and Y. Kawazore, Z. Phys. A **301**, 125 (1981).
- [20] R. Tamagaki and T. Takatsuka, Prog. Theor. Phys. **56**, 1340 (1976).
- [21] T. Takatsuka, K. Tamiya, T. Tatsumi and R. Tamagaki, Prog. Theor. Phys. **59**, 1933 (1978).
- [22] A. B. Migdal, Rev. Mod. Phys. **50**, 107 (1978).
- [23] F. Dautry and E. M. Nyman, Nucl. Phys. A **319**, 323 (1979).
- [24] D. V. Deryagin, D. Y. Grigoriev and V. A. Rubakov, Int. J. Mod. Phys. A **7**, 659 (1992).
- [25] E. Shuster and D. T. Son, Nucl. Phys. B **573**, 434 (2000).
- [26] B. Y. Park, M. Rho, A. Wirzba and I. Zahed, Phys. Rev. D **62**, 034015 (2000).
- [27] M. G. Alford, J. A. Bowers and K. Rajagopal, Phys. Rev. D **63**, 074016 (2001).
- [28] E. Nakano and T. Tatsumi, Phys. Rev. D **71**, 114006 (2005).
- [29] I. Giannakis and H. C. Ren, Phys. Lett. B **611**, 137 (2005).
- [30] K. Fukushima, Phys. Rev. D **73**, 094016 (2006).
- [31] D. Nickel, Phys. Rev. Lett. **103**, 072301 (2009); Phys. Rev. D **80**, 074025 (2009).
- [32] T. Kojo, Y. Hidaka, L. McLerran and R. D. Pisarski, Nucl. Phys. A **843**, 37 (2010).
- [33] S. Carignano, D. Nickel and M. Buballa, Phys. Rev. D **82**, 054009 (2010).
- [34] K. Fukushima, T. Hatsuda, Rept. Prog. Phys. **74**, 014001 (2011).
- [35] G. Gruner, Rev. Mod. Phys. **60**, 1129 (1988).
- [36] G. Gruner, Rev. Mod. Phys. **66**, 1 (1994).
- [37] Y. Kanada-En'yo and Y. Hidaka, Phys. Rev. C **84**, 014313 (2011).
- [38] J. Eichler, A. Faessler Nucl. Phys., A157,166 (1970).
- [39] N. Onishi, R.K. Sheline Nucl. Phys. A165, 180 (1971).
- [40] S. Takami, K. Yabamma, K. Ikeda, Prog. Theor. Phys. **96**, 407 (1996).
- [41] D. Robson, Phys. Rev. Lett. **42**, 876 (1979).
- [42] J.P.Elliott, J.A.Evans, E.E.Maqueda Nucl.Phys. A437, 208 (1985).
- [43] R. K. Sheline and K. Wildermuth, Nucl. Phys. **21**, 196 (1960).
- [44] H. Horiuchi and K. Ikeda, Prog. Theor. Phys. **40** (1968), 277[PTP].
- [45] Y. Funaki, T. Yamada, H. Horiuchi, G. Röpke, P. Schuck and A. Tohsaki, Phys. Rev. Lett. **101**, 082502 (2008).
- [46] Y. Funaki, T. Yamada, A. Tohsaki, H. Horiuchi, G. Röpke and P. Schuck, Phys. Rev. C **82**, 024312 (2010).
- [47] Y. Kanada-En'yo and H. Horiuchi, Prog. Theor. Phys. **93**, 115 (1995); Y. Kanada-En'yo, H. Horiuchi and A. Ono, Phys. Rev. C **52**, 628 (1995); Y. Kanada-En'yo and H. Horiuchi, Phys. Rev. C **52**, 647 (1995).
- [48] Y. Kanada-En'yo and H. Horiuchi, Prog. Theor. Phys. Suppl. **142**, 205 (2001).
- [49] Y. Kanada-En'yo M. Kimura and H. Horiuchi, C. R. Physique **4** 497 (2003).
- [50] Y. Kanada-En'yo, Phys. Rev. Lett. **81**, 5291 (1998).
- [51] Y. Kanada-En'yo, Prog. Theor. Phys. **117**, 655 (2007) [Erratum-*ibid.* **121**, 895 (2009)].
- [52] M.Chernykh, H.Feldmeier, T.Neff, P.von Neumann-Cosel and A.Richter, Phys. Rev. Lett. **98**, 032501 (2007).
- [53] D. M. Brink, International School of Physics "Enrico Fermi", XXXVI, p. 247 (1966).